Strain measurements on porous concrete samples for triaxial compression and extension tests under very high confinement

X H Vu*, **Y Malecot,** and **L Daudeville**
Université Joseph Fourier – Grenoble I, Laboratoire Sols, Solides, Structures – Risques, Grenoble, France

The manuscript was received on 31 March 2009 and was accepted after revision for publication on 16 July 2009.

DOI: 10.1243/03093247JSA547

Abstract: This article presents the production of strain measurements on porous concrete samples for use in triaxial compression and extension tests with a very high lateral confining pressure. When a massive concrete structure is subjected to severe loadings (e.g. rock falls, near-field detonations, and ballistic impacts), the material undergoes triaxial loading at a high confining pressure. To reproduce high levels of stress with well-controlled loading paths, static tests are carried out on concrete using a high-capacity triaxial press, called GIGA. This press allows the testing of concrete specimens (7 cm in diameter and 14 or 15.5 cm long) for levels of confining pressure ranging up to 850 MPa and axial stresses of up to 2.35 GPa. The porous characteristic of the material together with the high confining pressure require both developing a material protection device and building strain gauge-based instrumentation of unprecedented design for such confining pressures. In addition, the effect of pressure and other sources of error on strain and stress measurements are identified herein thanks to tests performed on model materials. This study shows that the effect of pressure on strain gauge measurements is negligible, whereas this same effect proves significant in the axial displacement measurement by means of a linear variable differential transformer (LVDT) sensor and must be taken into account therefore during the data processing phase. This article will present the initial results of triaxial compression tests conducted at high confining pressure on both dry and saturated concrete samples instrumented with gauges. It will also provide results of a triaxial extension test conducted at high confinement on dry concrete: a unique step in characterizing the triaxial behaviour of concrete. Moreover, it will be demonstrated that simultaneous axial strain measurements using gauges and the LVDT sensor serve to evaluate strain homogeneity of the sample tested at high confinement.

Keywords: concrete, triaxial compression test, triaxial extension test, high confinement, high stress, experimental procedure, strain measurements

1 INTRODUCTION

Concrete is the most widely used manufactured material in the world. In particular, it is employed in the building of highly sensitive infrastructure (civil engineering structures, dams, nuclear power plants, etc.). Its mechanical behaviour however is still rather poorly understood, especially under extreme loadings. When subjected to violent explosion or ballistic impact, concrete undergoes very severe triaxial loadings [**1**]. In exceptional cases, such an impact may cause complete perforation of the target. The validation of concrete behavioural models, which take the phenomena of fragile damage and irreversible strain in compaction into account simultaneously, thus requires test results capable of reproducing complex loading paths.

This triaxial behaviour can be identified under quasi-static conditions thanks to a triaxial press with high loading capacity, which allows for a homogeneous, well-controlled and precisely guided load-

**Corresponding author: Laboratoire Sols, Solides, Structures – Risques, Université Joseph Fourier – Grenoble I, Grenoble, 38041, France.*
email: vu@hmg.inpg.fr; vuxuanhong2003@yahoo.fr

ing. This type of test also makes it possible fully to instrument the studied object.

A high-capacity press, called GIGA, was specifically designed and installed in the 3S-R laboratory in collaboration with France's 'Centre d'Etudes de Gramat' (Délégation Générale pour l'Armement, French Ministry of Defence). This cooperative venture is part of a larger research project on the vulnerability of concrete infrastructure when subjected to impact. During the initial stage of this project, the joint mission focused on studying the quasi-static triaxial behaviour of concrete under very high confinement. In subsequent studies of this research, strain rate effects on concrete behaviour will be examined by means of both split Hopkinson pressure bar tests [**2**] and impact tests on targets.

Given the stress levels reached and the macroporous nature of the studied concretes, the introduction of triaxial testing has required the creation of experimental and instrumentation devices. This article will focus on the development and validation of such devices. In similar studies previously conducted on smaller samples at lower levels of stress and confinement [**1**, **3–6**], axial and orthoradial strain have been measured by means of a linear variable differential transformer (LVDT) displacement sensor. The pressure effect on an LVDT sensor measurement, however, was not discussed in any of these articles. Moreover, the moisture evolution of concrete samples during preparation before testing has not been evaluated in any of the preceding studies either. However, after the cement setting, concrete is a quasi-saturated material. In most cases, it is then submitted to an environment with lower relative humidity, such that a drying process occurs within the concrete. As the pore network of the cement matrix is very thin, this moisture transport proceeds very slowly and can be described using a diffusion-like equation [**7**]. The time required to reach moisture equilibrium varies with the square of the built structure thickness. Given that most sensitive concrete infrastructures, such as bridge piers, dams, and nuclear reactors, are very massive, their core can remain quasi-saturated most of their lifetime, while their facing dries very quickly. The saturation degree of the concrete is then an important parameter to look at to study the vulnerability of such massive infrastructures.

In this paper, the experimental device used to perform the current study will be described in section 2. Development of the experimental procedure for carrying out triaxial tests under very high confinement will be presented in section 3, which also focuses on the introduction of strain gauges for strain measurements of porous concrete samples under very high confinement. To the best of the current authors' knowledge, such an approach is unprecedented at such high confining pressures. This part of the paper will display the protective device for gauges and sample, along with the instrumentation set-up for saturated samples. The validation of this experimental procedure is the topic of section 4, which will also address the pressure effect on responses of the force sensor, extensometric gauges and the LVDT displacement sensor. Section 5 will offer the initial results of both the triaxial compression tests conducted on dry and saturated concretes and a triaxial extension test on dry concrete. This section will include a discussion to show how the simultaneous measurements of axial strain using a gauge and an LVDT sensor enable the evaluation of the strain homogeneity in the various samples. The paper closes with a presentation of the main conclusions from this study and the outlook for future work.

2 EXPERIMENTAL DEVICE

2.1 The triaxial cell

The high-capacity triaxial press, presented in Fig. 1, was especially designed and developed for this study. A cross-sectional view of the confinement cell is shown in Fig. 2, with the concrete sample being placed inside this cell. The press is able to load

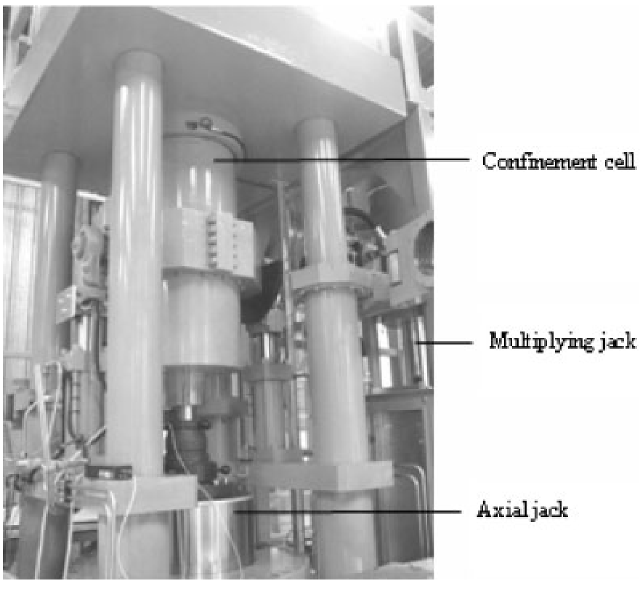

Fig. 1 The GIGA press

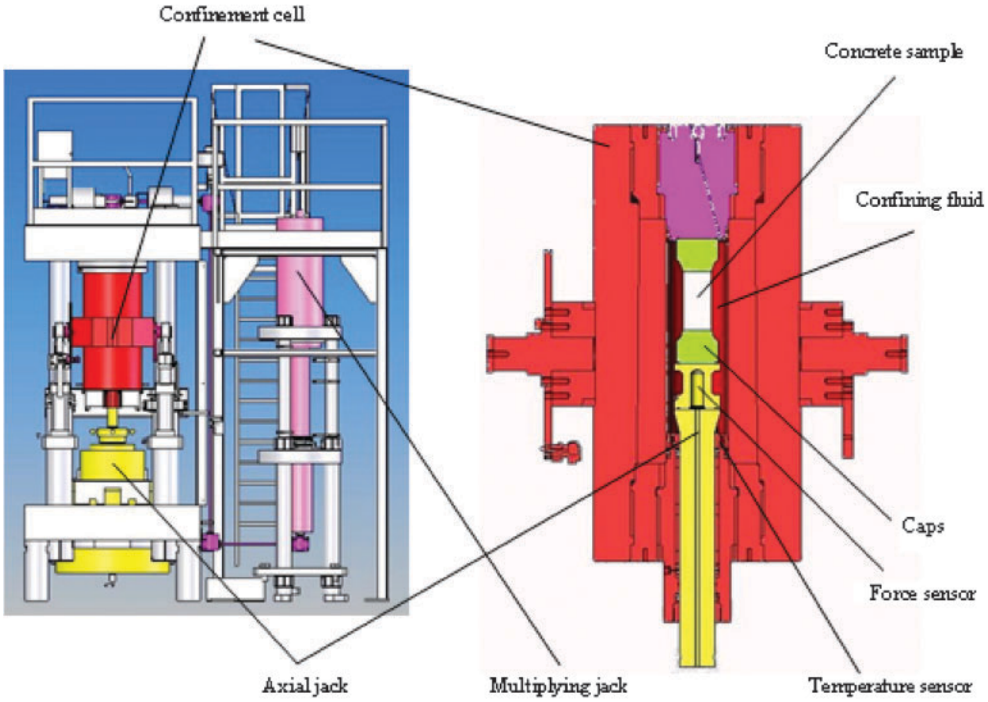

Fig. 2 General view of the GIGA press

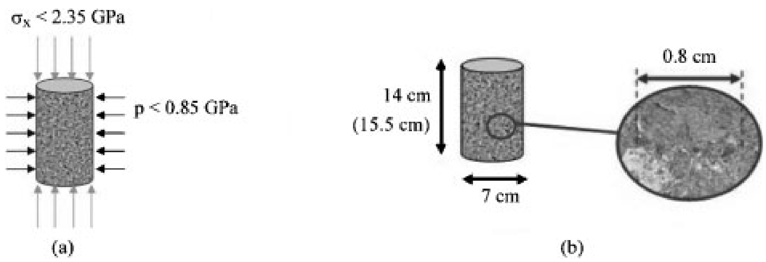

Fig. 3 (a) Maximum press capacity and (b) associated sample sizes of the triaxial cell

cylindrical concrete samples 7 cm in diameter and 14 or 15.5 cm long up to a confining pressure of 0.85 GPa and an axial stress reaching 2.35 GPa (see Fig. 3). The confining fluid, i.e. di-2-ethylhexyl azelate, a non-volatile organic, inert and slightly compressible liquid, is injected into the cell through an upper opening before being pressurized by means of a multiplying jack (Fig. 2, left). The jack is loaded under pressure by a primary hydraulic circuit up to 25 MPa, and its cross sectional ratio equal to 40 enables a pressure 40 times greater than that of the primary circuit inside the confinement cell to be obtained, i.e. reaching approx. 1 GPa. The difference between maximum capacity of the press (1 GPa) and its nominal pressure (850 MPa) stems from the charge loss within the pipe system for conveying fluid transmission from the multiplying jack output to the confinement cell.

The axial force is generated by a 13 MN jack placed underneath the cell (Fig. 2, right); it is transmitted to the sample via a piston that passes through the lower cell plug. A displacement sensor positioned inside the press is then used to guide axial displacement of the jack, while an axial force sensor and a pressure sensor placed within the confinement cell measure the sample stress state. Both the confining pressure and axial jack displacement are servo-controlled, which offers a variety of loading paths.

2.2 Loading path

The specimen and applicable loading are placed in a biaxial revolution. The specimen is loaded both hydrostatically and along its axis. The confining pressure and axial jack displacement are controlled and allow various loading paths to be generated; among these paths, hydrostatic compression, triaxial compression and triaxial extension were chosen for this study. They have been depicted in Fig. 4. For hydrostatic compression and triaxial compression, the specimen diameter was set at 7 cm and length at 14 cm. As for triaxial extension, specimen diameter remained 7 cm, while length was extended to 15.5 cm.

The hydrostatic loading consists of generating a confining pressure around the specimen, which has been placed between two caps and surrounded by a sealing membrane with respect to the confining fluid (see section 3.3). The confining pressure varies linearly over time, with a maximum rate of 1.67 MPa/s.

Hydrostatic tests were conducted on both polycarbonate and tungsten carbide samples for purposes of validating the experimental procedure. These tests were all driven at an identical rate of pressure increase (1.67 MPa/s). The unloading phase was executed using the inverse rate.

The triaxial loading is performed in two phases: hydrostatic and deviatoric. During the hydrostatic phase, the sample is loaded until it reaches the desired pressure, as defined by the user. The deviatoric phase, on the other hand, is conducted by imposing a constant displacement rate of the principal axial jack and then keeping the confining pressure constant. The triaxial compression tests were all carried out with identical rates of pressure increase (1.67 MPa/s) and principal jack displacement (20 μm/s, for a strain rate of approx. 0.14×10^{-3}/s with a 14 cm long specimen). It should be noted that the maximum deviator value has not been imposed, as a direct result of the test. The unloading phase once again proceeds using the inverse rate.

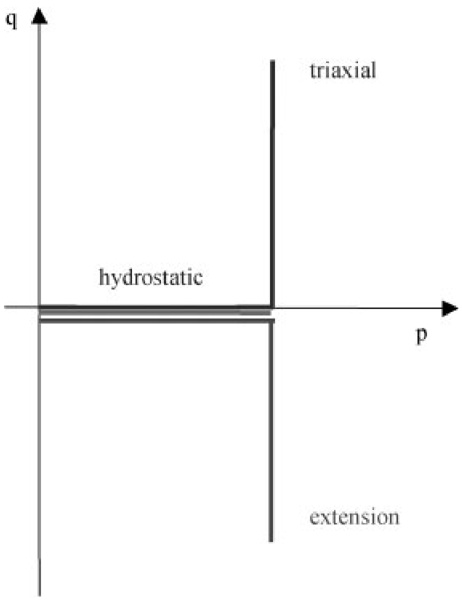

Fig. 4 Loading paths: hydrostatic compression, triaxial compression, and triaxial extension

The extension loading is applied to the sample hydrostatically until reaching the desired pressure, as established by the user (i.e. the hydrostatic phase); the axial stress is then released while maintaining a constant lateral stress (the extension phase). During the hydrostatic phase, the principal jack movement is determined by the confining pressure, whereas in the extension phase, the principal jack is moved while maintaining the confining pressure constant in order to reduce the deviatoric force to an actual test result value. The hydrostatic unloading test phase proceeds first by a decrease in lateral pressure around the sample and then by return of the principal jack. A triaxial extension test with a lateral pressure of 300 MPa was conducted as part of this study. During this test, the displacement rate (either up or down) of the principal jack was 2 μm/s, which translates into a strain rate of roughly 0.13×10^{-4}/s for a sample 15.5 cm long.

In this paper, compressive stresses and contraction strains are assumed to be positive; σ_x is the principal axial stress, p the pressure inside the confinement cell, σ_{m} the mean stress, and q the principal stress difference (deviatoric stress), i.e.

$$\sigma_{\mathrm{m}}=\frac{\sigma_x+2p}{3} \tag{1}$$

$$q=\sigma_x-p \tag{2}$$

3 TEST PROCEDURE DEVELOPMENT

Development of the experimental procedure, as presented in this section, will initially focus on both the characteristics and preparation of the concrete samples before discussing their instrumentation.

3.1 Characteristics and implementation of the studied concrete

This section begins by presenting the composition of the studied concrete; after this, the production, preparation and conservation of the concrete samples will be reviewed.

3.1.1 Composition of the studied concrete

The tested concrete displays a 28-day compressive strength of 30 MPa and a slump of 7 cm. The composition, mechanical and physical properties of this concrete are listed in Table 1. It should be noted that the very high-quality cement used, for purposes of greater control over material reproducibility, leads to a particularly low cement volume. Aggregate compounds containing 99 per cent quartzite are derived from natural deposits (i.e. rolled aggregates). The maximum aggregate size (8 mm) has been chosen on the basis of specimen diameter (70 mm). According to Yip and Tam [**8**], the effect of sample size can be neglected in simple compression for this maximum aggregate size. This conclusion is assumed to be valid as well in triaxial compression.

3.1.2 *Specimen production*

A production procedure for the concrete specimens was established with the aim of ensuring minimal variability in mechanical properties of the material. The concrete (R30A7) was cast in a parallelepiped mould in batches 13.5 l in volume. Concrete placement entails 30 s of vibration on a vibrating table. The concrete block, upon removal from the mould 24 h after casting, is conserved for 28 days in a saturated environment within plastic bags immersed in water, so as to insulate the concrete both physically and thermally. The block is then cored, cut and ground. All these machining stages are performed using water lubrication in order to avoid heating the concrete. The two sample faces are parallel to within 0.1 mm on a diameter of 70 mm. The observation of concrete specimens after machining (Fig. 5(a)) leads to the following findings: absence of surface cracking on the material surfaces; the cut aggregates and air bubbles also appear to be distributed over all specimen faces, thus indicating the lack of any concrete segregation problem.

Table 1(a) Composition properties of the reference concrete R30A7

0.5/8 "D" gravel (kg/m^3)	1008
1800 μm "D" sand (kg/m^3)	838
CEM I 52.5 N PM ES CP2 cement (Vicat) (kg/m^3)	263
Water (kg/m^3)	169
Density (kg/m^3)	2278
Water/cement ratio	0.64
Cement paste volume V_p (m^3/m^3)	0.252

3.1.3 *Preparation of the lateral sample surface*

Development of the gauge protective device, instrumented on concrete samples and tested at a high level of confinement (as described in section 3.4), shows the necessity of proceeding with a special preparation of the lateral sample surface.

In order to identify the most suitable material for filling large pores on the lateral sample surface, various materials (CHRYSOR C6120 resin, Sikadur-30 epoxy resin, Sikatop-SF-126 hydraulic mortar) have been tested. Given the characteristics of the studied concrete (Table 1), the Sikatop-SF-126 mortar [**9**], whose characteristics are similar to those of a normal concrete, has been chosen.

The step of preparing the lateral surface of a concrete sample begins by locating and opening underlying pores by lightly striking small surface pores with a sharp object, such as a needle or a nail or by using an electric milling machine. Both surface pores and the open underlying pores are then filled with fresh Sikatop-SF-126 mortar. After 24 h of open-air conservation, the mortar will have hardened and the lateral sample surface can be smoothed using

Table 1(b) Mechanical properties of the reference concrete R30A7

Average tested strength in uniaxial compression after 28 days of ageing (MPa)	28.6
Average slump measured using the Abrams cone (cm)	6.9
Volume of occluded air measured in fresh concrete (by use of an aerometer) (l/m^3)	34
Porosity accessible to water (%)	12

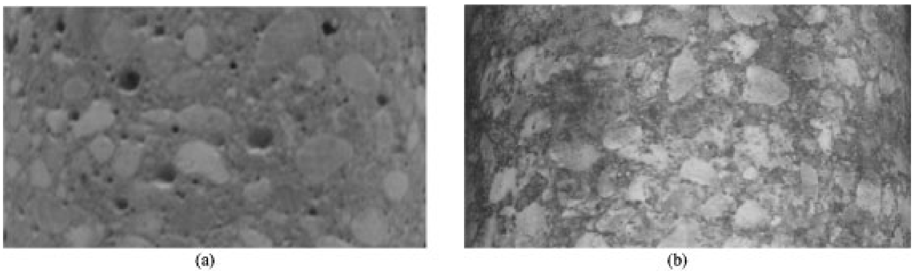

Fig. 5 Bare sample of (a) concrete R30A7 and (b) a sample of concrete R30A7 after the lateral surface preparation (i.e. a prepared sample)

sandpaper or a small electric sander. It can be observed that air bubbles on the lateral surface of the bare sample (Fig. 5(a)) have been completely filled by the mortar (Fig. 5(b)). A comparative study on sample mass variation before and after this preparation step has been performed; results show that the average quantities of concrete removed and mortar added for a 7×14 cm sample correspond respectively to 0.6 per cent and 0.8 per cent of sample weight. This finding therefore suggests that such a lateral treatment of the sample surface exerts only a negligible impact on concrete behaviour.

3.1.4 Concrete conservation conditions

The samples are held in water for about 4 months, in accordance with a conservation procedure. Two kinds of sample have been tested: dried and saturated.

After some 4 months of conservation in water, the 'dried specimens' are placed in a drying oven, at a temperature T of 50 °C and relative humidity (RH) of 8 per cent, for a period lasting between 3 and 6 months. Note that after 1 month of oven drying, the daily variation in sample mass does not exceed 0.1 per cent and can thus be considered stabilized.

According to the study conducted by Castellote *et al.* [**10**], when the cementitious matrix is dried at a temperature below 50 °C, decomposition of matrix components is very limited, with the major phenomenon here being the evaporation of free water within the cementitious matrix. The drying temperature of concrete (50 °C) is thus set so as to avoid damaging the concrete material.

The 'dried specimens' are then conserved in the ambient laboratory atmosphere (with T equal to about 18 °C and RH about 40 per cent) during the instrumentation procedure, which lasts roughly 3 days prior to testing. In such a sample the water mass in its volume typically increases by around 1.4 per cent after 3 days. The saturation ratio of the 'dried concrete' tested in this study is approximately 11 per cent. Note that the sample saturation ratio (Sr) is estimated from weight measurements as follows

$$\mathrm{Sr} = 1 - \frac{m_{\mathrm{sat}} - m}{\eta \left(m_{\mathrm{sat}} - m_{\mathrm{hyd}} \right)} \qquad (3)$$

where m is the sample mass, m_{sat} the mass of the saturated sample, m_{hyd} the mass of the saturated sample obtained from a hydrostatic weighing, and η the concrete porosity, assumed to be identical for each concrete sample (i.e. $\eta = 12$ per cent).

The 'saturated specimens' are conserved in water between 6 and 10 months before the test. For the delicate, saturated specimen, a specific strain gauge instrumentation procedure needed to be developed; this is described in section 3.6.

3.2 Strain measurement

The concrete sample is placed in the confinement cell (Fig. 2) by means of a mobile device (Fig. 6(a)). The sample, surrounded by a membrane, is then positioned between two loading heads made of tungsten carbide (Fig. 6(b)). The sample strain measurement is carried out using an axial LVDT

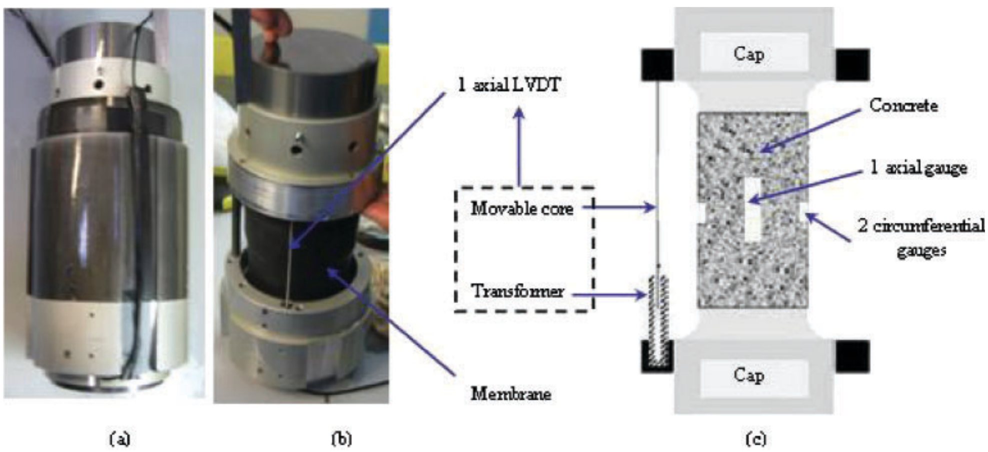

Fig. 6 (a), (b) mobile device and (c) schematic diagram of the strain measurement instrumentation applied to a specimen

sensor, an axial gauge and two circumferential gauges (Fig. 6(c)). The LVDT sensor used for this study, model 500X-3013 manufactured by the SCHAEVITZ Sensors Company, consists of a transformer and a movable magnetic core (Fig. 6(c)). Each part of the LVDT sensor is fastened onto a loading head through the aluminium mobile supports (Figs 6(b) and (c)). This sensor is capable of measuring relative displacement up to 50 mm. The axial gauge, bonded to the middle of the concrete sample, provides a local strain measurement. Note that during sample implementation on the mobile device, the LVDT sensor is positioned diametrically opposite the axial gauge. A comparison of axial strain, obtained respectively by the LVDT sensor and the axial gauge, allows evaluation of the sample strain homogeneity. The circumferential strain is measured using two diametrically opposed gauges. These two gauges serve to increase the probability of maintaining at least one measurement at the end of the test, while making it possible to verify strain homogeneity. To the best of the authors' knowledge, the use of gauges for triaxial testing on concrete at such high confinement levels is unprecedented.

The gauges used in this study, of the type EP-08-120-10CBE from Vishay Micro-Measurements, are 28 mm long, i.e. roughly four times the size of the largest aggregate in the concrete composition ($D_{\max} = 8$ mm). These gauges allow for strain measurements up to a 15 per cent elongation, which corresponds to expected strain at concrete failure under high confinement.

The GA2 type of glue produced by Vishay Micro-Measurements is used for bonding gauges and terminal strips onto the sample. This glue has been specially adapted for concrete bonding; it allows for sample strain measurement up to 15 per cent (i.e. strains measurable by the strain gauge fitted). The layer of GA2 glue at the interface between gauge and sample needs to be very thin so that the gauge response can represent the actual concrete strain [**11**]. Once gauges have been placed on the specimen using GA2 glue in the fresh state via the adhesive ribbons, a latex membrane (2 mm thick, 67 mm in diameter) is immediately placed around the sample. This membrane is positioned on the sample by use of a polyvinyl chloride (PVC) pipe and a vacuum system (Fig. 7(a)), which allows both spreading the fresh glue in a very thin layer and maintaining uniform pressure on the gauges throughout the time of glue setting (Fig. 7(b)). This set-up makes it possible to observe aggregates through the gauges (Fig. 7(c)).

3.3 Sealing membrane

The sealing membrane prevents the penetration of the confining fluid inside the porous concrete specimen during testing; such penetration modifies the mechanical characteristics of concrete. The membrane placed around the specimen is supported over a part of the loading heads.

The development process for a sealing membrane was complicated by the concrete porosity. During a test, when the specimen is under pressure, the presence of a surface pore or underlying pore generates high local punching stresses, which in turn cause perforation of the membrane owing to localized shear (Figs 8(a) and (b)). This perforation then leads to the infiltration of confining fluid into the specimen (Fig. 8(c)). Various material combinations involving latex (Fig. 8(b)), nitril (Fig. 8(c)),

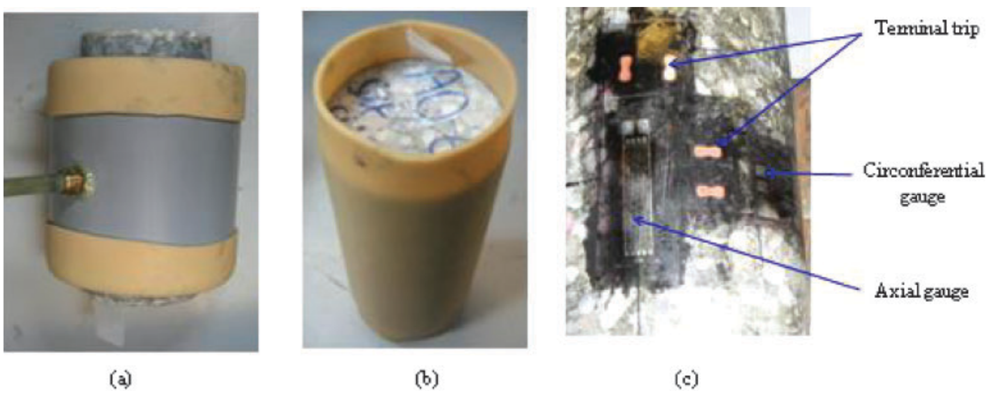

Fig. 7 Bonding of gauges onto the concrete sample: (a) application of the membrane on the sample using a prefabricated PVC pipe and a vacuum system; (b) maintaining a uniform pressure on the gauges during GA2 glue setting with a latex membrane (2 mm thick); (c) gauges and terminal strips bonded to the concrete sample

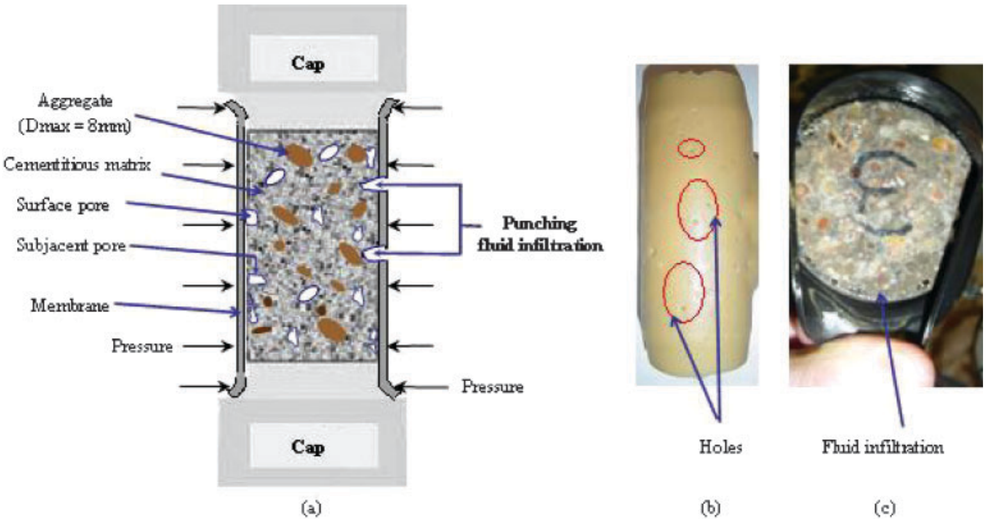

Fig. 8 (a) Perforation of the membrane due to surface and underlying macroscopic pores; (b) photograph showing perforation of the latex membrane following the test; (c) photograph showing infiltration of the confining fluid inside the specimen, surrounded by a nitril membrane, following the test

silicone and neoprene were tested during the membrane development stage. Latex was selected for its elasticity and shear strength. To facilitate fitting, a series of thin membrane layers are to be superimposed, which proves easier to install than a single thick membrane. Despite its strong mechanical characteristics, latex is chemically altered when coming into contact with the confining fluid. A neoprene membrane, placed over the latex layers, is thus introduced as chemical protection.

The validation tests conducted on membrane sealing consisted of comparing specimen weight before and after a test. Specimen variations of 15 to 20 g were recorded whenever sealing could not be ensured during the test; this mass corresponds to the quantity of confining fluid having infiltrated into the specimen. Variations of the order of 2 to 3 g are still observed on the membrane–specimen assembly when the confining fluid does not penetrate inside the specimen. The weighing of each element indicates that the confining fluid slightly alters the neoprene, without triggering any reaction with the latex. Regarding structural integrity of the membrane, the latex layers closest to the concrete surface are perforated, while those furthest away remain intact. The chosen optimal solution, depicted in Fig. 9, consists of 8 mm of latex covered by a 1 mm neoprene layer. Note that for all loading paths, the sealing between the loading heads and the top and bottom ends of the concrete specimen is ensured by the multi-layer membrane placed around the specimen and supported over a part of the loading heads. Furthermore, depending on the kind of test, either

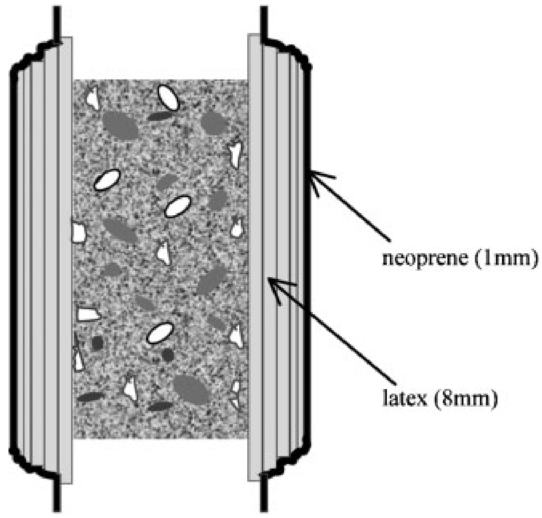

Fig. 9 Multi-layer membrane made of latex and neoprene (preferred solution)

there is no sealing between the loading heads and the piston (triaxial compression) or there is one (triaxial extension). In the first case, that means that the confining pressure applies on every face of the sample through the membranes or through the loading heads. In the second case, the confining pressure applies only on the lateral face of the sample which allows the imposition of an axial stress lower than the confining pressure (extension, see Fig. 15 and section 4.2 for details).

3.4 Gauge protective device

The multi-layer membrane ensures sealing of the specimen, yet does not prevent deterioration of both the gauges and gauge connection wires owing to punching (Figs 10(a) and (c)) when positioned above macroscopic or microscopic porosities beneath the surface. Such a condition leads to a loss of gauge signal during the test. To resolve this problem, two levels of protection have been introduced. The first consists of filling the large-diameter pores on the specimen lateral surface with mortar (see section 3.1.3), while the second calls for protecting the gauges with a semi-rigid shield that allows spreading the confining stress.

Several plastic shields composed of various materials (PVC, Veralite) and thicknesses were tested. Shields made of PVC both 2 mm thick (Fig. 11(a), shields 1 and 2) and 4 mm thick (Fig. 11(a), shield 3) were rejected owing to their very low shear strength. A shield with material of the type Veralite®200 and 2 mm thick (Fig. 11(a), shield 4) was then tested. This material [**12**], a transparent polyester within the family polyethylene terephthalate glycol (PETG), is flexible yet retains a very high tensile strength (approx. 51 MPa). Its inner surface state following the test (Fig. 11(a), shield 4) remains very regular, which serves to ensure proper stress distribution during the test. This material, made from a flat plate, has therefore been chosen to protect the gauges. Its cylindrical shape is produced by thermoforming on an aluminium cylinder of the same diameter as the specimen (Fig. 11(b)).

3.5 Installation of the wires and the membrane

The use of conventional wires or thin connection wires raises concerns (e.g. breaking of the wire with added pressure) (Fig. 10(c)). Single-strand, 0.2 mm

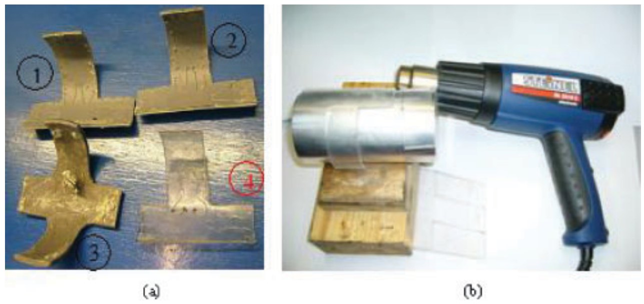

Fig. 11 (a) States of the shields (PVC (1, 2, 3), and Veralite (4)), after completion of the test; (b) thermoforming of the protective shield

wires have been used between the gauge and the terminal strips (Fig. 12(a)). Some tests have also shown that applied pressure could crush two soldered joints at the gauge output and thereby create a short-circuit. It thus proves essential to separate the single-strand wires to the greatest extent possible and introduce a minimum amount of solder. Single-strand wires 0.6 mm in diameter welded to the terminal strips are used to cross the protective shield (Figs 12(a) and (b)). Beyond the shield, the single-strand wires are connected to standard electric wires (Fig. 12(b)). Installation of the membrane on the sample has already been presented above (section 3.2, Fig. 7(a)). The insertion of wires through the membrane is performed using a hollow metal tube (Fig. 12(c)). The wires cross the latex layers and remain above the shield in relation to the specimen. The shield offers a flat surface that limits potential ruptures during test pressure variation. This passage of wires through the membrane constitutes one possible infiltration path for the confining fluid. An

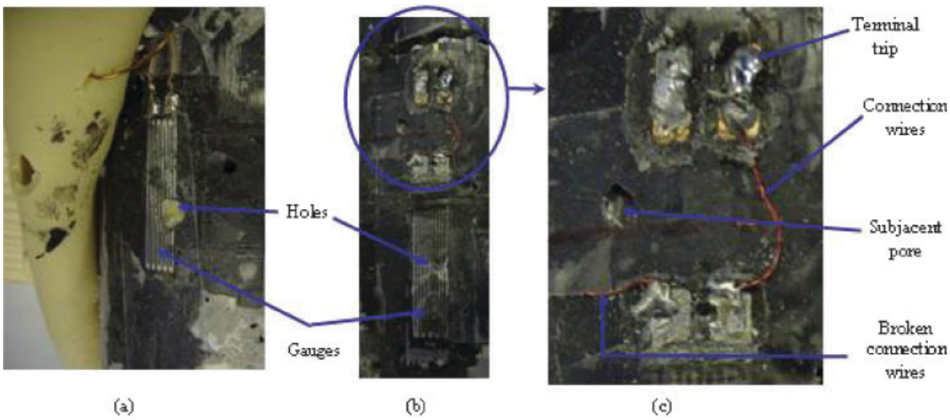

Fig. 10 Photographs illustrating the destruction of gauges and gauge connection wires: (a) gauge perforation owing to the presence of a macroscopic pore lying below the gauge; (b) gauge damage owing to the presence of a microscopic pore lying below the gauge; (c) close-up of the upper part of Fig. 10(b): rupture of gauge connection wires owing to the presence of a macroscopic pore lying below the wires

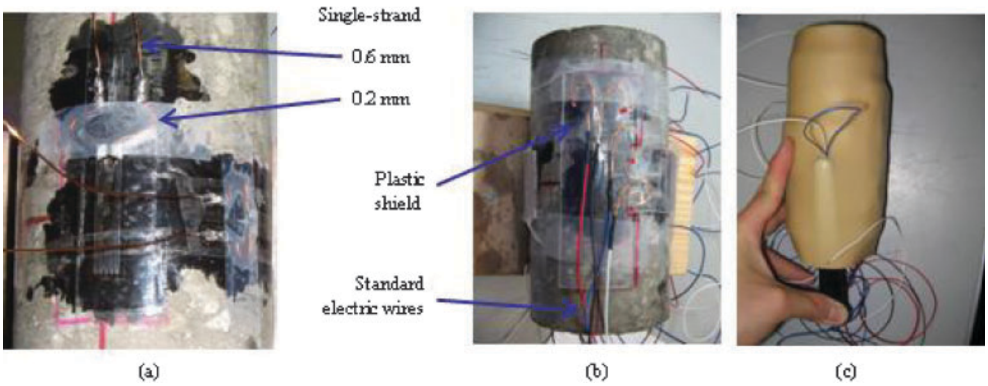

Fig. 12 (a) Gauge connection wires (two types of single-strand wire); (b) protective plastic shield of the type Veralite®200 and connection wires through the shield; (c) crossing of wires through the successive membrane layers

additional silicone seal, where wires exit the membrane, was therefore introduced. Figure 13 displays a schematic view of a specimen ready for testing. This solution allows the conduct of reliable tests at high confinement on porous concrete specimens and necessitates about 8 hours of work per specimen.

3.6 Preparation of saturated samples

One of the original features of this study pertains to controlling the degree of saturation of the test specimens. Preparation of the saturated sample requires additional precautions when bonding the gauges. Figure 14 shows the main steps involved in this preparation. Preparing the benchmarks used to track gauge bonding has been described previously. The sample is immersed in water in order to saturate it once again. For the gauge bonding phase, sample faces are insulated from ambient air by means of sealing plastic films, wet sponges (on the support surfaces) and a latex membrane (around the lateral surface) (see Fig. 14(a)). The latex membrane is locally cut for gauge installation (Fig. 14(a)). A thin layer of black GA2 glue is then placed on the areas reserved for gauge bonding. Once the last layer of glue has hardened, the gauges and their protective covering are set into place (Figs 14(a) and (c)). This additional layer of GA2 glue insulates not only the concrete surfaces from ambient air during curing, but also the gauges from wet concrete. This layer is necessary to obtain good gauge adhesion on the specimen and satisfactory operation during the test. A triaxial compression test could thus be conducted at a confining pressure of 200 MPa on a saturated specimen; the results of this test will be presented in section 5.1 below.

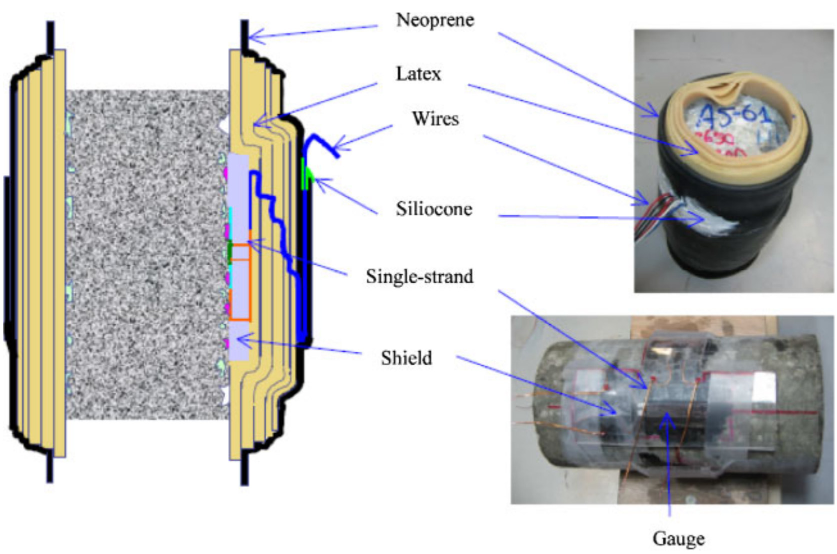

Fig. 13 Specimen ready to be tested

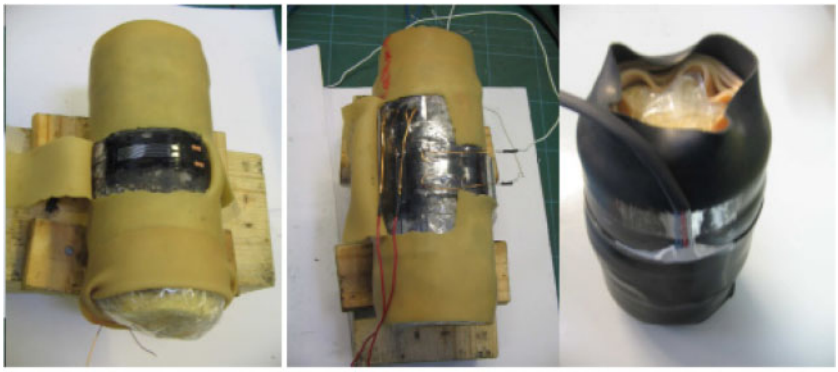

Fig. 14 Instrumentation procedure for gauges and membranes on a saturated specimen

4 TEST PROCEDURE VALIDATION

The objective of this section is twofold: to validate the choices made in the previous section, and to analyse the sources of error in the measurement of physical quantities.

4.1 Confining pressure measurement

The pressure sensor, installed at the entrance to the confinement cell, serves to determine pressure within the confinement cell. The manufacturer of the sensor has indicated a pressure measurement accuracy to within 1 per cent over the operating range, i.e. with an operating range of 1000 MPa, the maximum error will be 10 MPa. The sensor is to be calibrated, certified, and replaced annually. The pressure sensor will be considered as a reference sensor. The set of pressure corrections on the force sensor, on strain gauges or on the LVDT sensor will all assume that the pressure sensor signal remains accurate over time.

4.2 Axial force measurement

The force sensor enables the axial force applied to the specimen after treatment to be obtained. This sensor, positioned between the lower loading head and the piston (Fig. 15), is identical for both the compression test (hydrostatic and triaxial) and the triaxial extension test; its capacity reaches a maximum of 9 MN. The material is a metal that deforms elastically over the machine loading range. The force transmitted by the sensor is deduced from its strain.

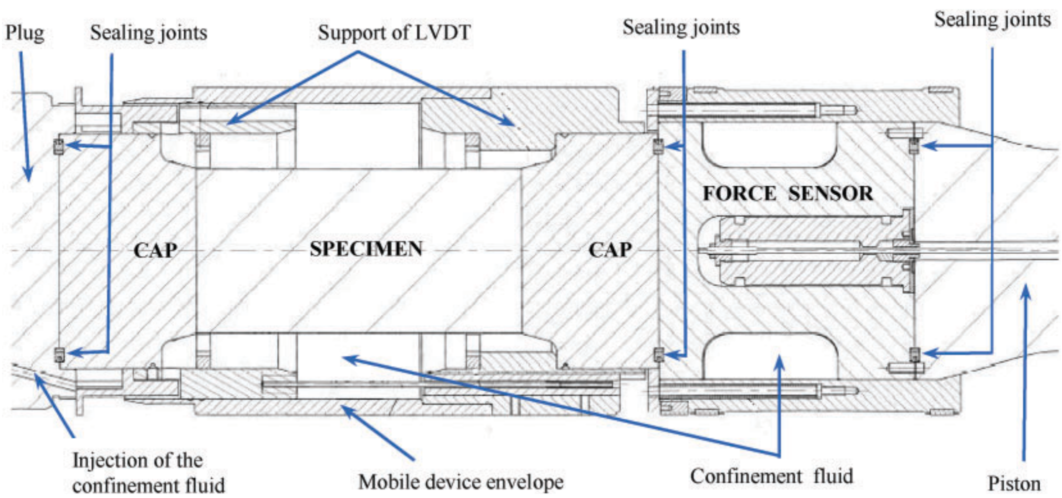

Fig. 15 Layout of the force sensor and the mobile device containing the specimen within the confinement cell of the GIGA press. For the triaxial extension test: presence of sealing joints between loading heads and plates; specimen length: 155 mm; total length of loading heads: 145 mm. For the compression test: absence of sealing joints between loading heads and plates; specimen length: 140 mm; total length of loading heads: 160 mm

For all loading paths, the confining fluid is not present at the interface between force sensor and piston, thanks to the presence of sealing joints (Fig. 15). For the extension loading, the presence of sealing joints prevents infiltration of the confining fluid at the interface between loading heads and loading plates as well as at the interface between the load sensor and piston (Fig. 15). For this loading, the two flat faces of the loading sensor are not subjected to confining pressure. For the compressive loading, no sealing joints have been placed between the loading heads and loading plates; for this loading, a flat face on the loading sensor, placed in contact with a loading head, has however been subjected to confining pressure. It should also be noted that the loading head length in the triaxial extension test (145 mm) is shorter than that in the compression test (160 mm), which leads to a difference between the specimen length in the triaxial extension test (155 mm) and that in the compression test (140 mm).

An examination is now made of the processing of axial force measurement for the case of the compressive loading. F_{mes}, which denotes the unprocessed response of the loading sensor, varies linearly with both the confining pressure and axial force transmitted by the piston. The axial force, F_x, is itself dependent on confining pressure, in accordance with the following formula

$$F_x = F_d + pS \tag{4}$$

where S is the specimen cross-section and F_d is the axial force after subtracting the confining pressure

In order to facilitate calibration, F_{mes} can be expressed as a function of F_d and p, according to the following equation

$$F_{mes} = \frac{F_d}{K_1} + K_2 p \tag{5}$$

where K_1 and K_2 are coefficients identified by the calibration steps.

The axial force F_x is thus deduced by

$$F_x = K_1(F_{mes} - K_2 p) + pS \tag{6}$$

It is noted that for the extension loading, axial force F_x (equation (6)) is calculated with a zero value for confining pressure p because the interfaces between loading heads and loading plates are not subjected to the confining pressure.

The coefficient K_1 is determined by means of a simple compression test at atmospheric pressure on a 2 MN calibration force sensor. Figure 16(a) displays the signal output by the force sensor F_{mes} (number of points – Npt) versus axial force F_x measured by the calibration force sensor.

The simple compression tests conducted on materials with very high elastic limits, such as tungsten carbide or steel, allow verification of force sensor linearity when the sensor is subjected to a very high axial force (up to 9 MN, i.e. the maximum capacity of the sensor). Tungsten carbide and steel are both isotropic homogeneous materials, in addition to being very rigid and subject to very low strains. A comparison of results from tests on tungsten carbide or steel, undertaken before and after tests performed at very high axial stresses on the concrete specimen, serves to track stability of the force sensor over time.

Simple compression tests on a tungsten carbide specimen have been carried out at different times.

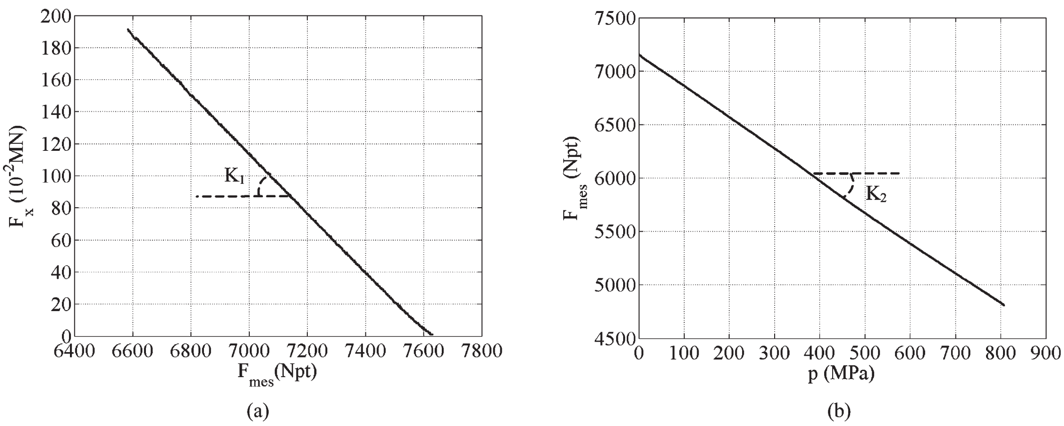

Fig. 16 Identification of coefficients: (a) K_1, and (b) K_2 for determining the axial force measured by the force sensor

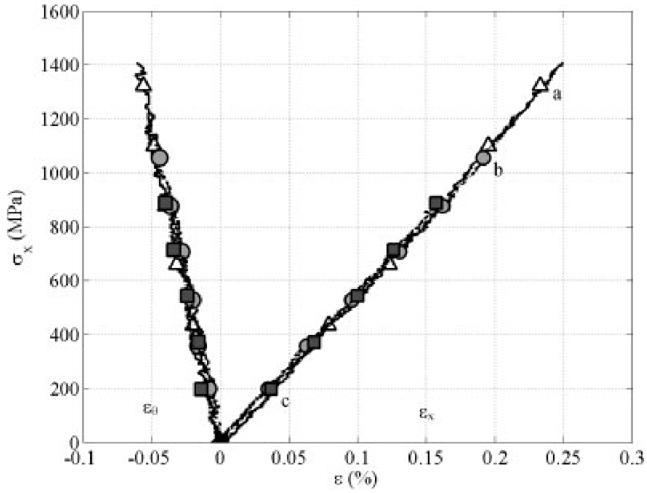

Fig. 17 Three simple compression tests: (a) triangle; (b) circle; (c) square, undertaken at different times and all using the GIGA press, on the same tungsten carbide specimen (included in the test loading); axial stress σ_x versus strain ε_x, ε_θ

The results of these tests are presented in Fig. 17 in terms of axial stress σ_x versus strain components ε_x and ε_θ. It can be observed that the curves (σ_x, ε_x) and (σ_x, ε_θ) nearly overlap. Note that one of these tests (test a) has yielded an axial stress level in the material of 1.4 GPa, i.e. close to maximum capacity of the GIGA press in terms of deviatoric stress ($q_{\max} = \sigma_{x\max} - p_{\max} = 1.5$ GPa) (see section 2.1). This finding indicates that the experimental device is able to carry out reproducible tests at high stress levels.

The coefficient K_2 is determined from a measurement of the confining pressure exposed to the force sensor in the hydrostatic test, i.e. when F_d equals zero (Fig. 16(b)). For each triaxial compression test, coefficient K_2 can easily be determined from the hydrostatic phase of this same test. The pressure effect on the force sensor at the time of testing has been fully taken into account.

4.3 Gauge-based strain measurements

In this section, the influence of both confining pressure and the protective device on gauge response will be examined.

4.3.1 *Influence of confining pressure on gauge response*

The influence of confining pressure on gauge measurements has been evaluated by means of tests conducted on a tungsten carbide specimen.

Influence of confining pressure on gauge strain. The strain ε_{mes}, given by a gauge, is computed from a measured tension U_{mes}

$$\varepsilon_{\text{mes}} = f(U_{\text{mes}}) \tag{7}$$

where f is a function which characterizes the sensitivity of the gauge. Besides, during a triaxial test, this measured strain ε_{mes} is the result of two kinds of strain

$$\varepsilon_{\text{mes}} = \varepsilon_{\text{specimen}} + \varepsilon_{\text{gauge}} \tag{8}$$

where $\varepsilon_{\text{specimen}}$ is the strain of the specimen on which the gauge is bonded and $\varepsilon_{\text{gauge}}$ is owing to the effect of the confining pressure on the gauge itself. Usually, if the confining pressure is not too important, $\varepsilon_{\text{gauge}}$ can be neglected and ε_{mes} is equal to $\varepsilon_{\text{specimen}}$, which is the physical quantity that is to be measured. To evaluate the influence of the confining pressure on gauge measurements, triaxial compression tests on a tungsten carbide specimen have been conducted.

Influence of confining pressure on gauge strain. The objective of this paragraph is to quantify $\varepsilon_{\text{gauge}}$ which depends only on the confining pressure and not on the material on which the gauge is bonded. To be as precise as possible, a hydrostatic test has been done on a tungsten carbide specimen the behaviour of which is both stiff and elastic (Fig. 18). Moreover, the elastic bulk modulus of tungsten carbide, K, has been identified from a simple compression test done on the same machine. Equation (8) can then be rewritten as

$$\varepsilon_{\text{gauge}} = \varepsilon_{\text{mes}} - \varepsilon_{\text{specimen}} \tag{9}$$

$$\varepsilon_{\text{specimen}} = \frac{p}{3K} = \frac{p(1-2\nu)}{E} \tag{10}$$

with elastic characteristics of tungsten carbide: $E = 562.5$ GPa and $\nu = 0.24$ (see section 4.2); and p, the confining pressure.

In spite of a high level of noise for ε_{mes} ($=\varepsilon_{x2}$, ε_{x3} or $\varepsilon_{\theta1}$), Fig. 18 shows that $\varepsilon_{\text{gauge}}$ is both negative and very low in absolute value (less than 0.02 per cent at 800 MPa). If the gauge is bonded onto a rigid specimen, the pressure would reduce the diameter of the gauge wire, leading to an increase in its resistance which explains this negative value. But whatever its sign is, the low value of $|\varepsilon_{\text{gauge}}|$ makes it negligible during triaxial test on concrete

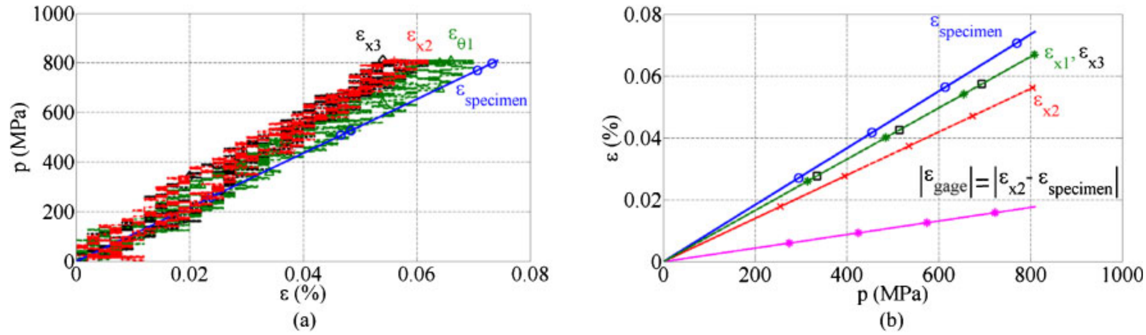

Fig. 18 Hydrostatic test on the tungsten carbide specimen: confining pressure p versus strains measured by two axial gauges (ε_{x2} and ε_{x3}) and by the circumferential gauge ($\varepsilon_{\theta 1}$); $\varepsilon_{\text{specimen}}$: specimen strain determined from elastic characteristics of the tungsten carbide, as identified during a simple compression test; $\varepsilon_{\text{gauge}}$: strain owing to the effect of the confining pressure on the gauge itself: (a) pressure versus strains; (b) deviation between gauge-measured strains and strains estimated from the simple compression test

($\varepsilon_{\text{specimen}} \sim 3$ per cent at 800 MPa). From now on in this article, ε_{mes} is equal to $\varepsilon_{\text{specimen}}$.

Influence of confining pressure on gauge sensitivity. The objective of this paragraph is to quantify the effect of the confining pressure on the function *f*. This influence is evaluated by means of triaxial compression tests conducted at various confining pressures on the same tungsten carbide specimen. This specimen has been instrumented with two diametrically opposite axial gauges and one circumferential gauge. The specimen axial strain corresponds to an average of the measurements recorded on two diametrically-opposite axial gauges. The deviatoric behaviour of a metallic material such as tungsten carbide (i.e. as measured by the stress deviator/strain deviator ratio) is independent of confining pressure.

Figure 19(a) shows the axial stress versus gauge-measured strains for both a simple compression test and a triaxial compression test at a confining pressure of 650 MPa. The deviatoric part of the material behaviour is indicated in Fig. 19(b). From Fig. 19(b), it can be observed that gauge responses during the deviatoric phase of the tests practically overlap for a confining pressure equal to either zero or 650 MPa. These tests demonstrate that gauge response (i.e. the function *f*) is not sensitive to confining pressure.

4.3.2 *Influence of the gauge protective device*

In order to assess the influence of the presence of both a shield and membranes on the gauge response, a series of hydrostatic tests were carried out on a polycarbonate specimen (Fig. 20) up to 700 MPa in three different configurations:

(a) Test 1: complete protective device;
(b) Test 2: protective device without membranes;
(c) Test 3: protective device without the shield.

Polycarbonate was chosen for the purpose of this evaluation for two reasons: it is isotropic, homo-

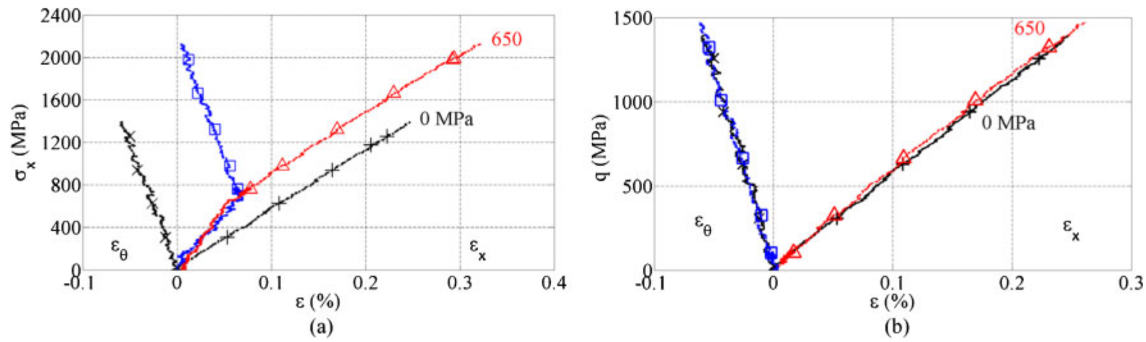

Fig. 19 Triaxial compression tests with confining pressures of 0 and 650 MPa on the same tungsten carbide specimen: (a) axial stress σ_x versus strain components ε_x, ε_θ; (b) deviatoric stress q versus strain components ε_x, ε_θ

Fig. 20 Polycarbonate specimen

geneous and nonporous; and its compressibility modulus is close to that of concrete.

A 1 mm thick neoprene membrane was used for all tests performed in order to keep the specimen centred within the mobile device and to protect the gauges from the confining fluid.

Both the gauges and glue used during these tests are identical to those applied to the concrete specimen (see section 3.3). The bonding of gauges with the GA2 glue, which has been specially designed for rough surfaces such as those found on concrete, to the very smooth surface of the polycarbonate specimen has required a supplementary preparatory step: the specimen was lightly scratched in areas where the gauges were to be bonded.

Figure 21 shows the pressure measurement versus strain measured using the axial gauge in various configurations. These curves practically overlap with one another. Besides, the bulk modulus *K*, determined from elastic characteristics (*E*, *v*), identified from a simple compression test, corresponds to the initial bulk modulus, in the pressure range from 0 to 200 MPa of the hydrostatic test, for which the material behaviour remains linear. The protective device therefore does not significantly influence gauge-based strain measurements.

4.4 Strain measurements by use of an LVDT sensor

This section is intended to identify error sources on the specimen axial strain measurement by introducing the LVDT sensor; the aim is to reveal the dual effect of loading head strain and of confining pressure on the LVDT sensor response.

4.4.1 Effect of loading head strain

The LVDT sensor enables the relative displacement of the upper loading head with respect to the bottom loading head to be measured. In order to evaluate the influence of loading head strain on the LVDT sensor response, a simple compression test was performed on a tungsten carbide specimen. Figure 22(a)

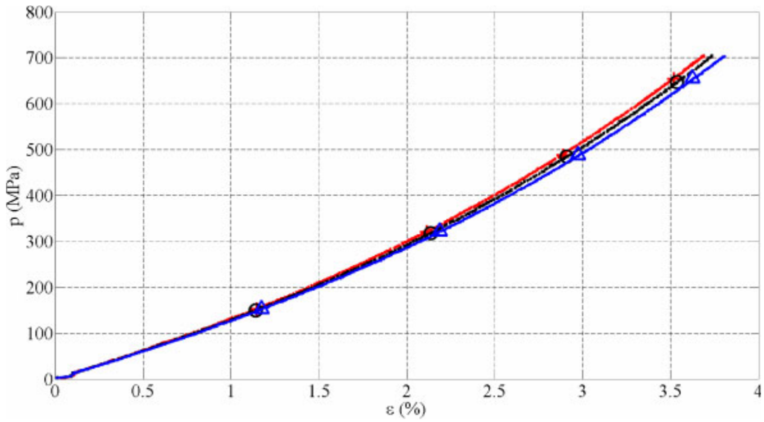

Fig. 21 Loading phases of hydrostatic tests performed on a polycarbonate specimen: influence of the shield and membranes on gauge-based strain measurements; (o, solid line) = complete protective device (test 1); (+, dot-dash line) = protective device without membranes (test 2); (triangle, dashed line) = protective device without the shield (test 3)

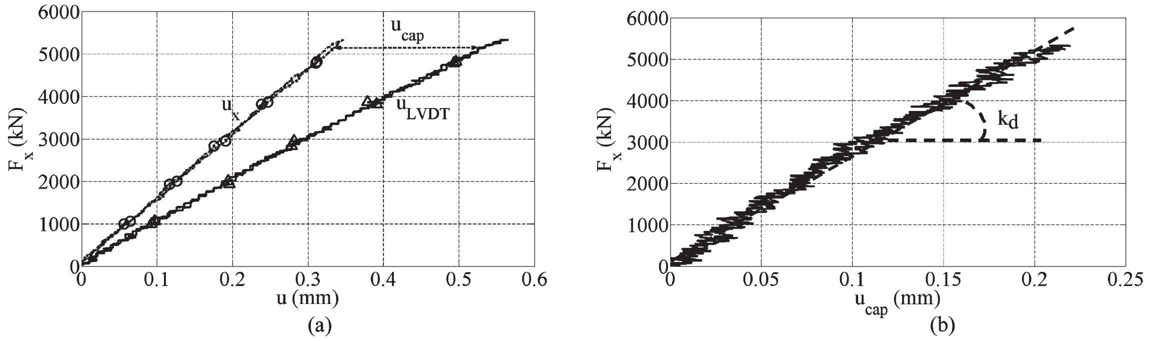

Fig. 22 Effect of loading head strain on LVDT sensor response: simple compression test on a tungsten carbide specimen: (a) axial force F_x versus specimen shortening u_x, as deduced from the axial gauge measurement (circle) and shortening measured by the LVDT sensor u_{LVDT} (triangle); (b) axial force F_x versus shortening of loading head parts to which LVDT sensor supports are fixed u_{cap} $(= u_{\mathrm{LVDT}} - u_x)$

presents the results of this test in terms of axial force F_x versus specimen shortening. This figure shows that the shortening measured by the LVDT sensor (u_{LVDT}) is greater than that measured by the gauge u_x. This result may be explained by the fact that the shortening measured by the LVDT sensor (u_{LVDT}) has been derived from the sum of specimen shortening and the shortening of those loading head parts to which the LVDT sensor supports are fixed (u_{cap})

$$u_{\mathrm{LVDT}} = u_x + u_{\mathrm{cap}} \tag{11}$$

where u_{LVDT} is the shortening of the LVDT sensor, u_x the specimen shortening, and u_{cap} the shortening of loading head parts to which the LVDT sensor supports are fixed.

Figure 22(b) indicates that a linear relationship exists between u_{cap} and the axial force, i.e.

$$u_{\mathrm{cap}} = F_x / k_{\mathrm{d}} \tag{12}$$

where k_{d} represents the stiffness of the loading head parts to which the LVDT sensor supports are fixed with respect to the axial force ($k_{\mathrm{d}} = 0.27 \times 10^5$ kN/mm).

4.4.2 Effect of confining pressure on the LVDT sensor

As for the gauges, the influence of confining pressure on measurements performed with the LVDT sensor was evaluated by introducing a hydrostatic test on a tungsten carbide specimen (Fig. 23). A comparison drawn between the gauge and LVDT sensor signals indicates that the influence of confining pressure on the LVDT sensor is indeed significant. The LVDT sensor measures an extension as the specimen contracts; this paradox is owing to the stiffness of the assembly containing the full LVDT sensor support (i.e. the LVDT sensor steel rod, two aluminium support parts and two tungsten carbide loading heads, see Fig. 6) with respect to confining pressure, which is lower than that of the tungsten carbide

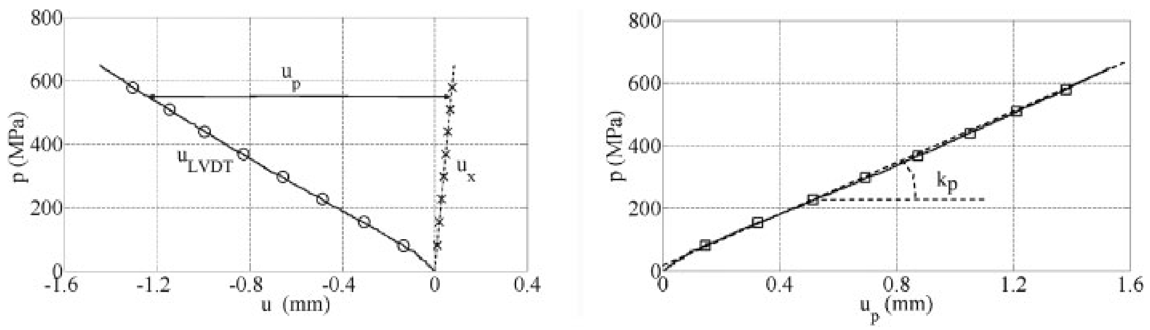

Fig. 23 Hydrostatic test on a tungsten carbide specimen: (a) confining pressure p versus LVDT sensor measurement u_{LVDT} (o) and specimen shortening u_x (x); u_p: elongation measured by the LVDT sensor as a result of the confining pressure effect; (b) confining pressure p versus elongation measured by the LVDT sensor as a result of the confining pressure effect

specimen. This paradox causes both the stem and LVDT sensor body to become relatively remote and thus yield an extension measurement. Such an effect is less distinct with concrete, a material much less rigid than tungsten carbide. It is still necessary however to take into consideration this phenomenon, which accounts for an error of approx. 1.1 per cent at a confining pressure equal to 650 MPa.

Figure 23(b) shows that the deviation between specimen shortening u_x and LVDT sensor measurement u_{LVDT} varies linearly with confining pressure, i.e.

$$u_{\mathrm{p}} = u_x - u_{\mathrm{LVDT}} = p/k_{\mathrm{p}} \tag{13}$$

where k_{p} is the coefficient correlated with stiffness of the assembly of LVDT sensor support parts with respect to confining pressure ($k_{\mathrm{p}} = 0.42\times10^3$ MPa/mm; u_x is the specimen shortening as determined from the elastic characteristics of tungsten carbide (identified by means of a simple compression test – $u_x = L\varepsilon_{\mathrm{specimen}}$, see section 4.3.1); and L is the specimen length.

As for the gauges, the confining pressure effect on LVDT sensor sensitivity is evaluated by means of triaxial compression tests conducted at various confining pressures on a tungsten carbide specimen.

Figure 24(a) displays the LVDT sensor response versus axial stress for both a simple compression test and a triaxial compression test at a confining pressure of 650 MPa. Figure 24(b) then shows LVDT sensor shortening versus deviatoric stress. From Fig. 24(b), it can be observed that the slopes measured in the deviatoric phase of the tests are identical for confining pressures of either zero or 650 MPa. This finding indicates that LVDT sensor sensitivity remains independent of confining pressure.

Given the elements presented in the previous sections, specimen shortening u_x can now be deduced from the LVDT sensor measurement u_{LVDT} by applying the following relation

$$u_x = u_{\mathrm{LVDT}} - u_{Fx,\mathrm{p}} \tag{14}$$

$$u_{Fx,\mathrm{p}} = (F_x - pS)/k_{\mathrm{d}} - p/k_{\mathrm{p}} \tag{15}$$

where u_{LVDT} is the unprocessed response obtained by the LVDT sensor measurement; $u_{Fx,\mathrm{p}}$ is the correction to be taken into account on the LVDT sensor measurement; p and F_x are respectively the confining pressure and axial force; S is the specimen cross-section; k_{d} the coefficient representing stiffness of the loading head parts to which the LVDT sensor supports are fixed with respect to the axial force; k_{p} is the coefficient relative to stiffness of the entire assembly of LVDT sensor support parts with respect to confining pressure.

For tests carried out with the GIGA press, the identified values of k_{p} and k_{d} equal 0.27×10^5 (kN/mm) and $0.42\cdot10^3$ (MPa/mm), respectively.

Figure 25 provides the successive steps involved in LVDT sensor measurement signal processing for a triaxial compression test conducted at a confining pressure of 650 MPa on a tungsten carbide specimen. This figure shows that after correction, the axial strain measurement, as deduced from the LVDT sensor response u_x/L, is perfectly consistent with gauge measurements that require absolutely no corrections.

5 RESULTS OF TESTS CONDUCTED ON CONCRETE SPECIMENS

5.1 Triaxial compression

A test performed at a confining pressure of 650 MPa on a dry concrete specimen (Sr = 11 per cent) and

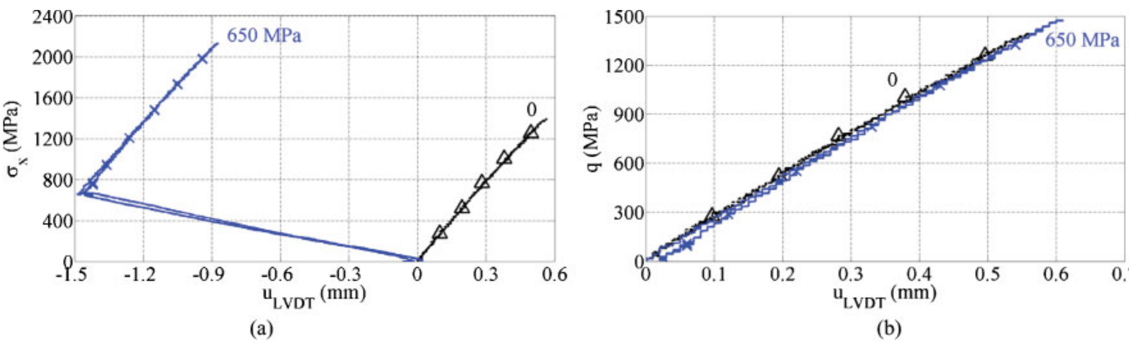

Fig. 24 Triaxial compression tests with confining pressures of 0 MPa (triangle) and 650 MPa (x) on a tungsten carbide specimen: (a) axial stress σ_x versus LVDT sensor response; (b) deviatoric stress q versus LVDT sensor response for the deviatoric phase

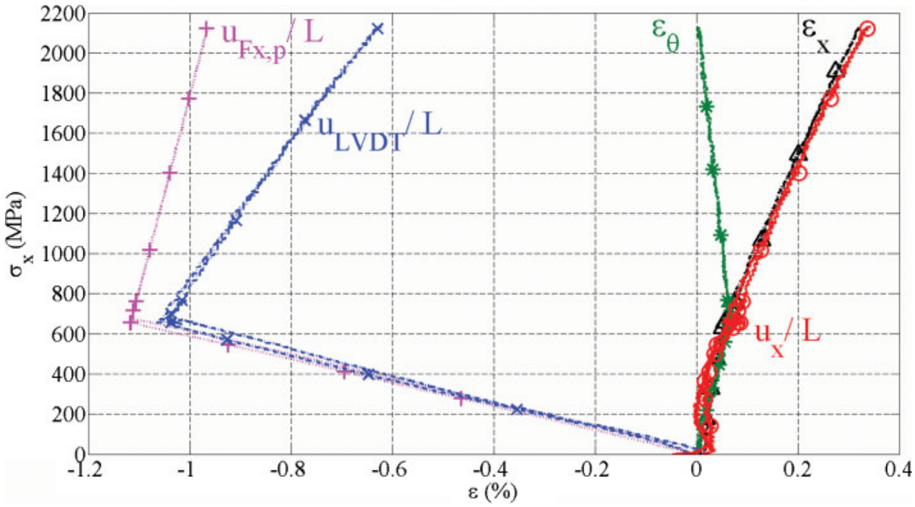

Fig. 25 Triaxial test on a tungsten carbide sample: x = unprocessed LVDT measurement (u_{LVDT}/L); + = correction ($u_{Fx,p}/L$); o = sample shortening after correction (u_x/L); L = tested sample length; triangle = gauge-based axial strain measurement ε_x; * = gauge-based circumferential strain measurement ε_θ

another test at a confining pressure of 200 MPa on a saturated concrete specimen (Sr = 100 per cent) will be presented herein for illustrative purposes. Figure 26 shows the evolution in axial stress σ_x and deviatoric stress q versus strain components ε_x and ε_θ. The axial strains represented have been obtained from the respective measurements of the LVDT sensor and gauge, while the circumferential strain

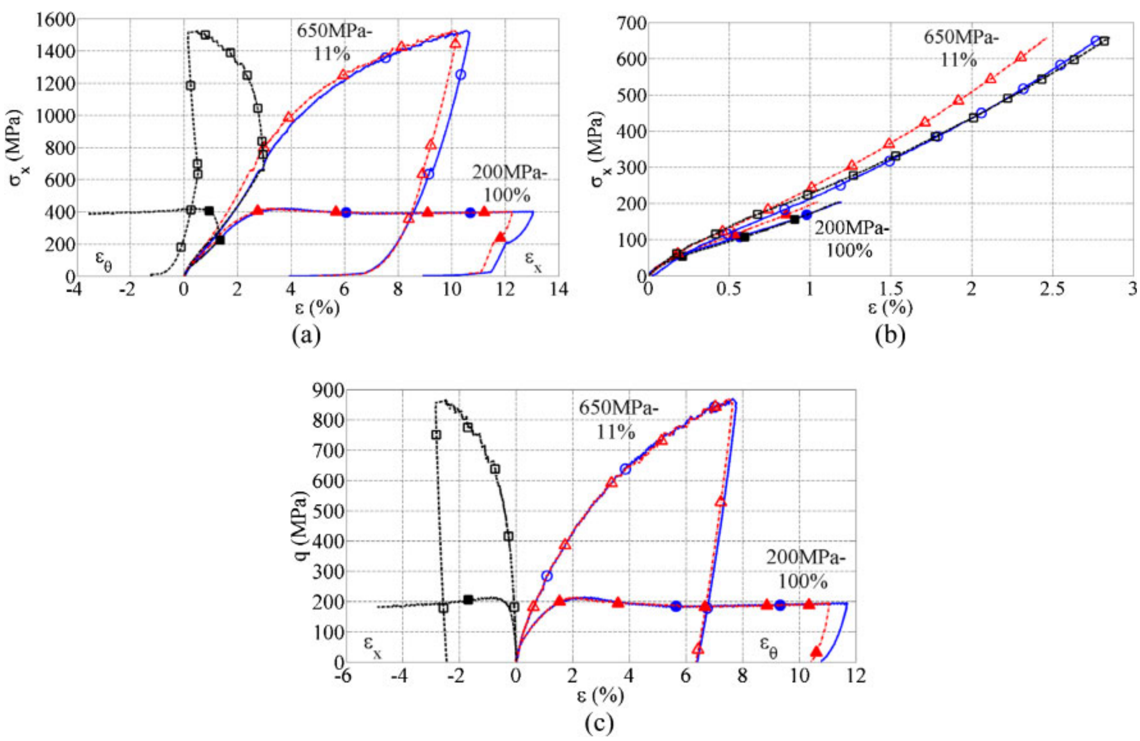

Fig. 26 Triaxial compression tests on concrete for various saturation rates (Sr = 11 per cent (unfilled symbols) and 100 per cent (filled symbols)) as well as at various confining pressures (p = 200 MPa and 650 MPa); axial LVDT (full line, o); axial gauge (dot-dash line, triangle); circumferential gauge (dashed line, square): (a) axial stress σ_x versus strain components ε_x and ε_θ; (b) close-up of the hydrostatic loading phases; (c) deviatoric stress q versus strain components ε_x and ε_θ

corresponds to an average of the measurements recorded on two diametrically opposite gauges.

For each test specimen, Fig. 26(a) exhibits a good level of consistency between the axial strain measured by the gauge and that measured by the LVDT sensor, up to a very high strain level. However, even if the friction between the loading heads and the ends of the concrete specimens is reduced to a minimum, it exerts an effect on the homogeneity of the stress state in the specimen. During the hydrostatic part of the test the specimen is compressed in every direction so that the friction is in the opposite direction compared with that which is usually observed in the conventional unconfined compression test. This negative friction reduces the confinement in the concrete near the loading heads. Then the concrete in the middle of the specimen deforms slightly less than the concrete in both ends of it. The axial strain obtained by the gauge is slightly lower than that obtained by the LVDT sensor during the hydrostatic part of the test (see test at 650 MPa in Fig. 26(b)). On the other hand, during the deviatoric phase of the test, due to Poisson's effect, the friction acts in the opposite direction. Strains in both ends of the specimen are lower than those in the middle of the specimen. The axial strain measured by the gauge is then slightly higher than that measured by the LVDT sensor (see test at 200 MPa on Fig. 26(c)). Because of these two compensated effects, the more the confining pressure is important, the more the strain seems to be homogeneous in the specimen during the triaxial test (see also Fig. 30). This indicates that the strain state of the specimens remains quite homogeneous, even at very high strain levels (i.e. $\varepsilon_x > 10$ per cent). Furthermore, during the hydrostatic phase of testing (Fig. 26(b)), it can also be observed that the axial and circumferential strain curves lie extremely close to one another. The strain state of concrete is thus nearly isotropic under hydrostatic loading.

The test carried out on the dry specimen, at a confining pressure of 650 MPa, reveals a hardening behaviour (Fig. 26(a) and (c)). For this test, no peak stress can be reached prior to unloading. Note that the axial stress of this specimen climbs to a level of 1500 MPa as axial strain reaches about 10 per cent. The test on the saturated sample, at a 200 MPa confining pressure, displays a ductile behaviour with a peak stress followed by a horizontal plateau (Fig. 26(a) and (c)).

Figure 27 presents the evolution in mean stress σ_m versus volumetric strain ε_v for these same tests. The mean stress σ_m and volumetric strain ε_v are calculated from measurements described in the previous section by using equations (1) and (16)

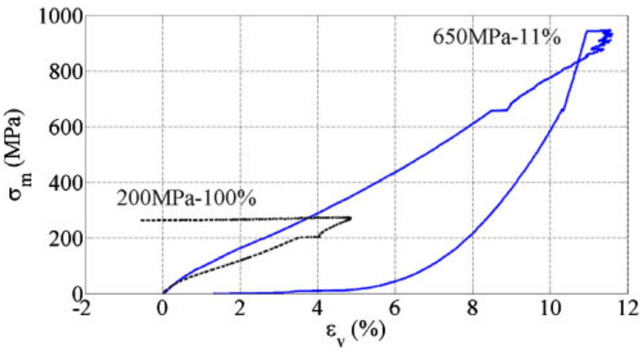

Fig. 27 Triaxial compression tests on concrete: mean stress σ_m versus volumetric strain ε_v; $p = 650$ MPa and $Sr = 11$ per cent (solid line); $p = 200$ MPa and $Sr = 100$ per cent (dashed line)

$$\varepsilon_v = \varepsilon_x + 2\varepsilon_\theta \tag{16}$$

The first part of the curves drawn in Fig. 27 corresponds to the hydrostatic loading phase. For each test specimen, it can be observed that behaviour is linear up to a mean stress of around 50 MPa. Beyond this linear phase, a progressive decrease occurs in the concrete tangent modulus, and this may be attributed to gradual damage to the cementitious matrix owing to hydrostatic compression. The linear phase continues until it reaches an inflection point located at a mean stress level between 100 and 200 MPa, which marks the transition towards a steady increase in tangential stiffness. This last phase of behaviour is explained by the specimen volume decrease, which in turn leads to material densification and thus an increase in stiffness. This behaviour of concrete under hydrostatic loading is consistent with reports from the literature for mortar [**13**, **14**] or for concrete at lower confining pressure levels [**1**, **3–6**, **15**].

The second part of the curves in Fig. 27 corresponds to the deviatoric phase of loading. It should be remarked that when approaching the peak stress, the concrete behaviour turns to expansion. The transition point from material contraction to dilatancy corresponds to the state of maximum volumetric contraction that the concrete is capable of reaching; this point defines a strain limit state of the concrete. For the saturated specimen tested at a confining pressure of 200 MPa, the contraction–dilatancy transition point is very distinct and nearly coincides with the appearance of peak stress (i.e. the stress limit state). For the dry specimen tested at

650 MPa however, the contraction–dilatancy transition point is much less marked. The appearance of expansion lies well below the maximum axial stress level, which moreover has not been reached during this test. The final part of the curves corresponds to the unloading phase (only that of the 650 MPa test is shown). A very high level of nonlinearity can be observed at the completion of unloading; at this point, the residual volumetric strain of the concrete returns to less than 2 per cent. This substantial decrease in tangential modulus is probably attributable to damage of the cementitious matrix when the granular skeleton, which essentially remains elastic, returns to its original form.

5.2 Triaxial extension

A triaxial extension test conducted at a confining pressure of 300 MPa on a dry concrete specimen (Sr = 11 per cent) will now be illustrated. Figure 28 shows the evolution of axial stress σ_x and deviatoric stress q versus strain components ε_x and ε_θ. The axial strains have been obtained from measurements by both the LVDT sensor (ε_{x1}) and gauge (ε_{x2}); while the circumferential strains are measured by circumferential gauges ($\varepsilon_{\theta 1}$ and $\varepsilon_{\theta 2}$). Owing to technical problems associated with the experimental devices used, the axial gauge measurement for strain levels above 1 per cent has had to be discarded (Figs 28(a) and (c)); moreover, the measurement of one of the circumferential gauges ($\varepsilon_{\theta 2}$) is very noisy compared with the other ($\varepsilon_{\theta 1}$) (Fig. 28(b)). Despite this noisy measurement on one circumferential gauge, it can still be observed that circumferential strains, obtained by two diametrically opposed gauges, are quite close and consistent (Figs 28(b) and (d)).

During the hydrostatic phase of the test (Figs 28(c) and (a)), the curves of axial and circumferential strains are very close to one another. The strain state of the concrete is thus nearly homogeneous and

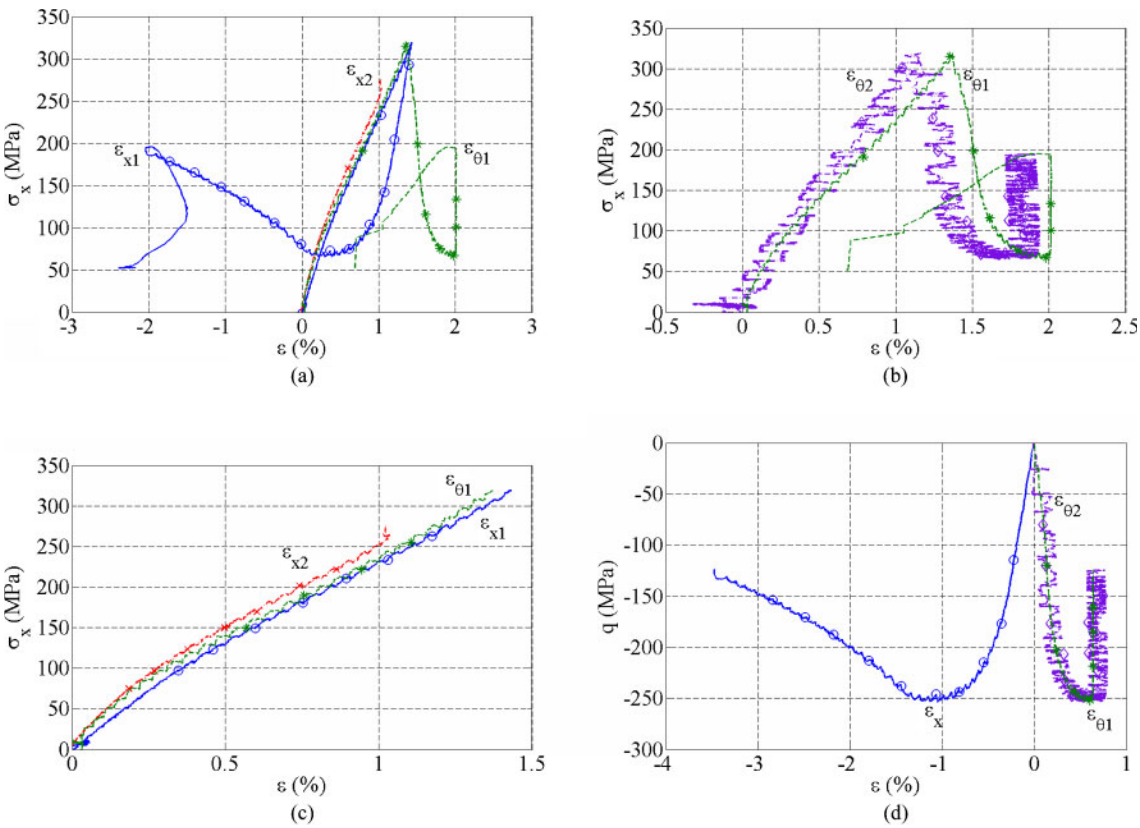

Fig. 28 Triaxial extension test on a dry concrete specimen at 300 MPa of confining pressure; axial strain obtained with LVDT sensor – ε_{x1} (full line, o); axial strain measured by the gauge - ε_{x2} (dash-dot line, x); circumferential strain measured by gauge 1 –$\varepsilon_{\theta 1}$ (dashed line, *); circumferential strain measured by gauge 2 – $\varepsilon_{\theta 2}$ (dash-dot line, diamond). (a) Axial stress σ_x versus strain components ε_{x1}, ε_{x2}, and $\varepsilon_{\theta 1}$. (b) Axial stress σ_x versus strain components $\varepsilon_{\theta 1}$ and $\varepsilon_{\theta 2}$. (c) Axial stress σ_x versus strain components ε_{x1}, ε_{x2}, and $\varepsilon_{\theta 1}$ (close-up on the hydrostatic loading phases of the test). (d) Stress deviator q versus strain components ε_{x1}, ε_{x2}, and $\varepsilon_{\theta 1}$

isotropic under hydrostatic loading. The axial and circumferential strains measured during this test are also consistent with those observed in the triaxial compression test at 650 MPa on the dry concrete specimen (see section 5.1).

The extension phase of the test (Figs 28(d) and (a)) indicates an axial extension and a circumferential contraction of the specimen, which is the opposite of what has been observed for a classical triaxial compression test. During this phase, the material tangential stiffness gradually decreases with an increase in the material axial strain. A minimum stress threshold for the material can be observed within the expansion phase of the test at an axial stress of around 65 MPa (Fig 28(a)) or −253 MPa of deviator (Fig. 28(d)). This threshold corresponds to the minimum stress state that the material is able to undergo in triaxial extension and serves to define the stress limit state of the material.

The test unloading phase (Fig. 28(a)) begins with the gradual reduction in confining pressure on the specimen lateral surfaces, until reaching zero pressure by keeping the same imposed axial displacement of the specimen. Once the confining pressure on the lateral surfaces has reached zero, the imposed axial displacement of the concrete specimen gradually decreases until the end of the test. This unloading phase initially produces an axial contraction and circumferential extension (the phase of decreasing confining pressure on the lateral surfaces) and then an axial extension and near-zero variation of specimen circumferential strain (the phase of gradually decreasing imposed axial displacement). It may be noted at this point that beyond the minimum stress threshold, the axial strain evolution (ε_{x1}) is consistent with the axial stress evolution. The circumferential strain variation however is not entirely consistent with axial stress evolution. The evolution in circumferential strain is next to zero over the two following portions of the stress–strain curve (Fig. 28(a)): between the minimum stress threshold and the end of test loading (first part), and between the beginning of the decrease in imposed axial displacement on the specimen and the end of the test (second part). As a matter of fact, the circumferential strain measurement, as obtained from the gauges, is a local measurement, while the axial strain measurement obtained with the LVDT sensor is global. The inconsistent evolution between axial stress and circumferential strains may be correlated with a material localization when the material is being loaded in an imposed displacement beyond its stress limit state.

Figure 29 presents the evolution in mean stress σ_{m} versus volumetric strain ε_{v} for the same test. σ_{m} and ε_{v} are calculated from measurements described in the previous section by applying equations (1) and (16). Owing to technical problems associated with both axial gauge (ε_{x2}) and circumferential gauge 2 ($\varepsilon_{\theta 2}$) measurements, the axial strain ε_{x1} obtained by the LVDT sensor and circumferential strain $\varepsilon_{\theta 2}$ obtained from circumferential gauge 1 have been selected in order to calculate the volumetric strain (equation (16)).

The first part of the curve in Fig. 29 corresponds to the hydrostatic loading phase. Concrete behaviour under hydrostatic loading is entirely consistent with what has been observed in the triaxial compression test on the dry concrete specimen R30A7 (Sr = 11 per cent) (see section 5.1). It should be noted that at a mean stress of 300 MPa, volumetric strain in the concrete specimen, as obtained from the triaxial compression test and triaxial extension test respectively, are nearly identical (approx. 4 per cent). This finding confirms the reproducibility of concrete behaviour under hydrostatic loading as well as the reliability of specimen preparation for the various tests.

The second part of the curve in Fig. 29 corresponds to the extension phase. The first observation points to a gradual decrease in mean stress versus a limited evolution in the concrete volumetric contraction. When approaching the minimum stress threshold, concrete behaviour turns to expansion. Similarly to the triaxial compression test, the transition point from material contraction to dilatancy defines a strain limit state for the material. This contraction–expansion transition point is very easily identified and coincides with the appearance of the minimum stress threshold (i.e. the stress limit state). Beyond the contraction–expansion transition of the

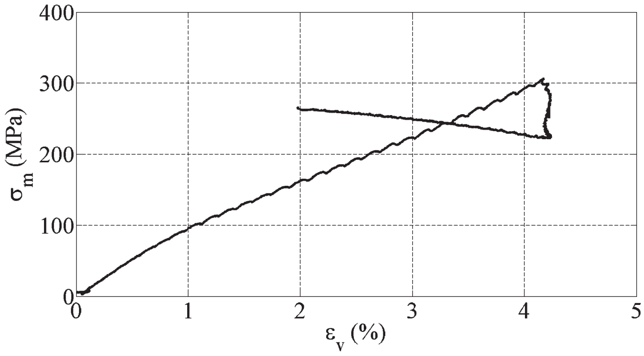

Fig. 29 Triaxial extension test on dry concrete at a confining pressure of 300 MPa: mean stress σ_{m} versus volumetric strain ε_{v}

material and until entering the test unloading phase (around a mean stress of 265 MPa), a gradual increase in mean stress, or rather a gradual increase in the deviator versus a decrease in material volumetric strain (i.e. material dilatancy), can be observed. Also note that during this phase, an axial elongation of the specimen occurs along with a circumferential strain that nearly equals zero. This phenomenon may be correlated as well with a material localization when the material has been loaded beyond its stress or strain limit state.

5.3 Strain homogeneity

The comparison between axial strain measured by the gauge (ε_{x2}) and that measured with the LVDT sensor (ε_{x1}) allows the evaluation of the strain homogeneity of specimens. Figure 30 shows that for specimens tested at high confining pressures (100 MPa, 200 MPa, and 650 MPa), the strains measured by the gauge remain very consistent with those deduced from the LVDT sensor up until test completion. This strain homogeneity reveals uniform specimen damage. For tests at lower confining pressures (0 MPa and 50 MPa) however, the signals are only consistent over the initial loading phase. Beyond the peak stress, i.e. at an axial strain of 0.2 per cent in simple compression and 2 per cent with a confining pressure of 50 MPa, the strain measured by the gauge diverges from that output by the LVDT sensor. This phenomenon, typical of a material with softening behaviour, is indicative of strain localization in the specimen at peak stress.

6 CONCLUSIONS AND OUTLOOK

The context of this study relates to the identification of concrete behaviour under extreme loadings. In order to reproduce high levels of stress with well-controlled loading paths, static tests on concrete specimens using a very-high-capacity triaxial press have been conducted. This paper has focused

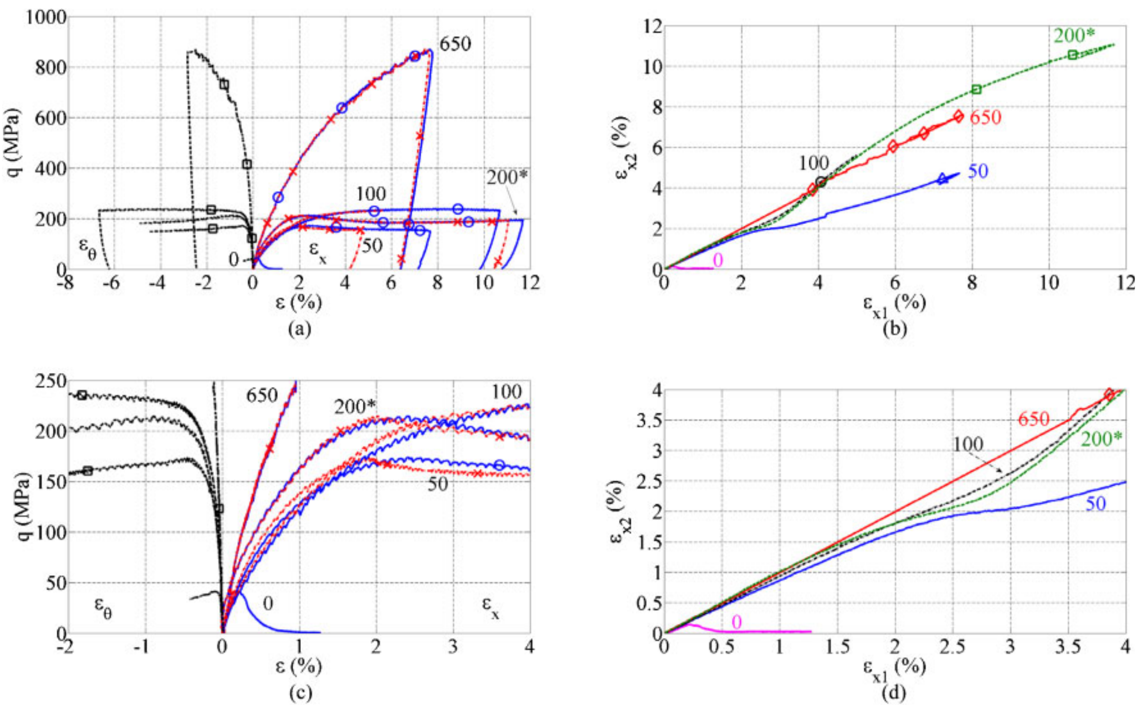

Fig. 30 Triaxial compression tests with confining pressures ranging from 0 to 650 MPa on dry concrete specimens (Sr = 11 per cent),except for the specimen marked with an (*) and tested at 200 MPa (saturated, Sr = 100 per cent): Deviatoric part of the behaviour: (a) deviatoric stress q versus strain components ε_x and ε_θ; strain deduced from the LVDT sensor (solid line, o); axial strains measured by gauges (dot-dash lines, x); circumferential strains measured by gauges (dashed lines, square); (b) axial strain of the specimen measured by gauge ε_{x2} versus that obtained by the LVDT sensor ε_{x1} for the loading phase of the deviatoric part of material behaviour; $p = 0$ MPa (solid line, no marker); 50 MPa (solid line, triangle); 100 MPa (dot-dash line, circle); 200 MPa (dashed line, square); 650 MPa (solid line, diamond); (c) close-up of Fig. 30(a); (d) close-up of Fig. 30(b)

specifically on developing and validating strain measurements by means of gauges and the LVDT displacement sensor on concrete specimens through performing tests with very high confining pressures.

A concrete specimen production and preparation protocol has also been developed. Strain measurements by use of gauges bonded to the concrete could be undertaken by means of special preparation of the specimen lateral surface in addition to introducing a protective device. Sealing problems, owing to the presence of macroscopic concrete pores responsible for membrane perforation and confining fluid infiltration into the specimen, have been resolved thanks to development of a protective multi-layer membrane. Hydrostatic tests, conducted on a polycarbonate specimen, have shown that this protective device does not exert a significant impact on strain measurements using gauges. This paper has also effectively demonstrated the possibility of performing strain measurements with gauges by controlling the degree of concrete saturation (from dry to saturated concrete). The effect of confining pressure on strain measurement has been highlighted through triaxial compression tests on a tungsten carbide specimen. While the pressure effect on strain measurement using gauges may be neglected, pressure does however strongly modify the LVDT sensor measurement, which requires correction.

The initial triaxial compression and extension tests conducted on concrete enable the validation of the experimental device developed herein. The axial and circumferential strain measurements of the concrete specimen under high confinement also allow the characterization of the specimen behaviour. The volumetric behaviour curve yields an evaluation of concrete compaction as well as its strain state limit. A comparison drawn between the axial strain obtained by gauge measurements and that deduced from the LVDT sensor measurement also offers an evaluation of strain homogeneity along with the possible detection of the localization phenomenon.

This study has demonstrated the possibility of performing, in a most reliable manner, triaxial compression and extension tests at high confinement pressures on porous concrete specimens with a controlled degree of saturation. Thanks to the innovative experimental device developed during this study, the initial experimental campaigns focusing on the influence of loading path [**16**], the water/cement ratio [**17**, **18**], degree of saturation [**19**] have been undertaken and have yielded unprecedented results. This device has also allowed the study of both concrete damage [**20**] and concrete behaviour [**21**] under high stress. Future improvements to the GIGA experimental device will consist of draining excess water and measuring pore pressure, in an effort to better quantify the effect of degree of concrete saturation on its behaviour under high confinement.

ACKNOWLEDGEMENTS

The GIGA press has been installed in the 3S-R laboratory within the framework of a cooperative agreement signed with France’s Délégation Générale pour l’Armement (CEG, DGA, French Ministry of Defence). This research has been performed thanks to financial support received from the ‘Centre d’Etudes de Gramat’ (CEG, DGA). The authors would like to thank Dr Eric Buzaud and Dr Christophe Pontiroli (CEG) for giving technical and scientific advice.

REFERENCES

1 **Warren, T., Fossum, A.,** and **Frew, D.** Experimental investigation of size effect in concrete fracture under multiaxial compression into low-strength (23 MPa) concrete: target characterization and simulations. *Int. J. Impact Engng*, 2004, **30**, 477–503.

2 **Hopkinson, B.** A method of measuring the pressure in the deformation of high explosives or by the impact of bullets. *Phil. Trans R. Soc.*, 1914, **A213**, 437–452.

3 **Akers, S. A.** and **Phillips, B. R.** Concrete modelled as an inhomogeneous material: numerical simulations of contact detonation charges. In 18th International Symposium on *The military aspects of blast and shock*, Oberjettenberg, Germany, 2004.

4 **Schmidt, J. M.** *High pressure and high strain rate behavior of cementitious materials: experiments and elastic/viscoplastic modeling*, doctoral dissertation, University of Florida, USA, 2003.

5 **Schmidt, J. M., Cazacu, O.,** and **Green, M. L.** Experimental and theoretical investigation of the high-pressure behavior of concrete. *Int. J. Numer. Analytical Meth. Geomech.*, 2008, **33**(1), 1–23.

6 **William, E. M., Akers, S. E.,** and **Reed, P. A.** Constitutive models for the triaxial behavior of concrete. Geotechnical and Structures Laboratory, 2005, U.S. Army. Report no. ERDC/GSL TR-05-16.

7 **Baroghel-Bouny, V., Mainguy, M., Lassabatere, T.,** and **Coussy, O.** Characterization and identification of equilibrium and transfer moisture properties for ordinary and high-performance cementitious ma-

terials. *Cement and Concrete Res.*, 1999, **29**, 225–1238.

8 **Yip, W. K.** and **Tam, C. T.** Concrete strength evaluation through the use of small diameter cores. *Mag. Concrete Res.*, 1995, **40**(143), 99–105.

9 Sikatop-SF-126, Technical notice of the mortar Sikatop-SF-126, document no. 6.53, version no. 146, 2007, Sika France S.A., 2007, available from www.sika.fr. In French.

10 **Castellote, M., Alonso, C., Andradea, C., Turrillas, X.,** and **Campoc, J.** Composition and microstructural changes of cement pastes upon heating, as studied by neutron diffraction. *Cement and Concrete Res.*, 2004, **34**, 1633–1644.

11 Strain Gage applications with M-bond AE-10, AE-15 and GA-2 Adhesive Systems, Instruction Bulletin B-137, document no. 11137, Vishay Micro-Measurements, Revision 05 April 2005.

12 Veralite®200, Technical sheet of Veralite®200 (PETG - Polyéthylène Téréphtalate Glycol), Product of I.P.B., Waregem, Belgium, available from http://www.ipb.be.

13 **Bazant, Z. P., Bishop, F. C.,** and **Chang, T. P.** Confined compression tests of cement paste and concrete up to 300 Ksi. *ACI Journal*, 1986, **33**, 553–560.

14 **Burlion, N., Pijaudier-Cabot, G.,** and **Dahan, N.** Experimental analysis of compaction of concrete and motar. *Int. J. Numer. Analytical Methods in Geomech.*, 2001, **25**, 1467–1486.

15 **Sfer, D., Carol, I., Gettu, R.,** and **Etse, G.** Study of the behavior of concrete under triaxial compression. *J. Engng Mech.*, 2002, **128**(2), 156–163.

16 **Gabet, T., Malecot, Y.,** and **Daudeville, L.** Triaxial behavior of concrete under high stresses: Influence of the loading path on compaction and limit states. *Cement and Concrete Res.*, 2008, **38**(3), 403–412.

17 **Vu, X. H., Malecot, Y., Daudeville, L.,** and **Buzaud, E.** Effect of the water/cement ratio on concrete behavior under extreme loading. *Int. J. Numer. Analytical Methods in Geomech.*, 2009, in press. DOI: 10.1002/nag.796.

18 **Vu, X. H., Malecot, Y., Daudeville, L.,** and **Buzaud, E.** Comportement du béton sous fort confinement: effet du rapport eau/ciment. *Eur. J. Environ. Civil Engng*, 2008, **12**(4), 429–457. DOI: 10.3166/ejece.12.429-457. In French.

19 **Vu, X. H., Malecot, Y.,** and **Daudeville, L.** Experimental analysis of concrete behavior under high confinement: effect of the saturation ratio. *Int. J. Solids Structs*, 2009, **46**, 1105–1120. DOI: 10.1016/j.ijsolstr.2008.10.015 (b).

20 **Poinard, C., Malecot, Y.,** and **Daudeville, L.** Damage of concrete in a very high stress state: experimental investigation. *Mater. Structs*, 2009. DOI 10.1617/s11527-008-9467-6.

21 **Dupray, F., Malecot, Y., Daudeville, L.,** and **Buzaud, E.** A mesoscopic model for the behaviour of concrete under high confinement. *Int. J. Numer. Analytical Methods in Geomech.*, 2009. DOI: 10.1002/nag.771.

APPENDIX

Notation

Variables

E, K, ν	Young's modulus, compressibility modulus, Poisson's ratio
f	function characterizing the sensitivity of the gauge
F_{d}	axial force after subtracting the confining pressure
F_{mes}	unprocessed response of the loading sensor
F_{x}	axial force
k_{d}	coefficient representing stiffness of the loading head parts to which the LVDT sensor supports are fixed with respect to the axial force
k_{p}	coefficient representing stiffness of the loading head parts to which the LVDT sensor supports are fixed with respect to confining pressure
K_1, K_2	coefficients linked to the force sensor, identified by the calibration steps
L	sample length
m	sample mass
m_{hyd}	mass of the saturated sample from hydrostatic weighing
m_{sat}	mass of the saturated sample
p	confining pressure
$q = \sigma_x - p$	deviatoric stress (deviator)
S	specimen cross-section
Sr	concrete saturation ratio $\mathrm{Sr} = 1 - \frac{m_{\mathrm{sat}} - m}{\eta\left(m_{\mathrm{sat}} - m_{\mathrm{hyd}}\right)}$
u_{cap}	shortening of loading head parts to which the LVDT sensor supports are fixed
$u_{\mathrm{Fx,p}}$	correction to be taken into account on the LVDT sensor measurement
u_{LVDT}	unprocessed response obtained by the LVDT sensor measurement
u_x	specimen shortening
U_{mes}	measured tension of the gauge
$\varepsilon_{\mathrm{gauge}}$	strain owing to the effect of the confining pressure on the gauge itself

ε_{mes}	specimen strain measured by gauge
$\varepsilon_{\text{specimen}}$	specimen strain
$\varepsilon_{\text{v}} = \varepsilon_x + 2\varepsilon_\theta$	volumetric strain
ε_x	mean axial strain
$\varepsilon_{x1}, \varepsilon_{x2}, \varepsilon_{x3}$	axial strains obtained respectively with measurements of the LVDT sensor, of the axial gauge 1 and of the axial gauge 2
ε_θ	mean circumferential strain
$\varepsilon_{\theta 1}, \varepsilon_{\theta 2}$	circumferential strains obtained respectively with measurements of the circumferential gauge 1 and of the circumferential gauge 2
η	concrete porosity accessible to water
$\sigma_{\text{m}} = \frac{\sigma_x + 2p}{3}$	mean stress
σ_x	axial stress

Designation of the concretes

Dried concrete – Sr = 11 per cent
Saturated concrete – Sr = 100 per cent

Sign conventions

$\varepsilon \geqslant 0$	during contraction
$\sigma \geqslant 0$	during compression

Abbreviations

LVDT	linear variable differential transformer

650 MPa–11 per cent: triaxial test, conducted at 650 MPa of confining pressure on a concrete sample displaying a saturation ratio of 11 per cent (p = 650 MPa, Sr = 11 per cent)

200 MPa–100 per cent: triaxial test, conducted at 200 MPa, of confining pressure on a saturated concrete sample (p = 200 MPa, Sr = 100 per cent)